Soil Moisture Change Monitoring from C and L-band SAR Interferometric Phase Observations

Sadegh Ranjbar, Mehdi Akhoondzadeh, Brian Brisco, Meisam Amani, *Senior Member, IEEE*, and Mehdi Hosseini

***Abstract*—The soil moisture changes (ΔM_v) have a significant influence on forestry, hydrology, meteorology, agriculture, and climate change. Interferometric synthetic aperture radar (InSAR), as a potential remote sensing tool for change detection, was relatively less investigated for monitoring this parameter. DInSAR phase (φ) is sensitive to the changes in soil moisture (M_v), and thus, can be potentially used for monitoring ΔM_v. In this article, the relations between φ and ΔM_v over wheat, canola, corn, soybean, weed, peas, and bare fields were investigated using an empirical regression technique. To this end, dual-polarimetric C-band Sentinel-1A and quad-polarimetric L-band uninhabited aerial vehicle synthetic aperture radar (UAVSAR) airborne datasets were employed. The regression model showed the coefficient of determination (R^2) of 40% to 56% and RMSE of 4.3 vol.% to 6.1 vol.% between the measured and estimated ΔM_v for different crop types when the temporal baseline (ΔT) was very short. As expected, higher accuracies were obtained using UAVSAR given its very short ΔT and its longer wavelength with R^2 of 47% to 59% and RMSE of 4.1 vol.% to 6.7 vol.% for different crop types. However, using the Sentinel-1 data with the long ΔT and shorter wavelength (5.6 cm), the accuracies of ΔM_v estimations decreased significantly. The results of this study demonstrated that using the φ information from Sentinel-1 data is a promising approach for monitoring ΔM_v at an early growing season or before the crop starts growing, but using L-band SAR data and lower temporal baselines are recommended once the biomass increases.**

***Index Terms*—Change detection, interferometric phase, soil moisture, synthetic aperture radar (SAR).**

I. Introduction

INTERFEROMETRIC Synthetic Aperture Radar (InSAR) is a remote sensing technique for monitoring a broad range of phenomena, such as permafrost studies [1], analysis of groundwater-related subsidence [2], [3], volcanology [3], and tectonics [3]–[5]. Measuring the topography of a surface and the displacement of the earth surface over time are other applications of InSAR [3], [6], [7]. Recently, this technique has been used to estimate soil moisture (M_v) as a change in the characteristic of the surface [8]–[10]. However, InSAR technique was relatively less investigated for monitoring M_v compared to other microwave methods such as theoretical and physical models [11], [12].

Researchers reported movements of surface that were related to watering when they were working with SEASAT data in 1989, confirming a relationship between M_v and interferometric phase (φ) [13]. Thus, the φ that is obtained by combining two radar images is an important parameter for soil moisture change (ΔM_v) estimation [8], [9], [14]. In addition to ΔM_v, there are other factors that affect the phase between the two observations, including deformations, vegetation, wind speed/direction, and atmosphere condition [12], [14]. Although these effects have been recognized at least since 1989, the studies on ΔM_v monitoring using the φ and coherence are limited to a few studies that have been mainly conducted using the laboratory experiments [15]–[18], as well as a few studies on using the airborne or satellite data [19]–[23]. Researchers have been interested in studying the effect of ΔM_v on φ for two main reasons, 1) correcting the corresponding error in displacement estimation, and 2) using InSAR technique for monitoring ΔM_v.

Interferometric phase (φ), coherence magnitude (γ), and closure phase or phase triplet (Ξ) are three differential InSAR (DInSAR) parameters that are used for M_v monitoring [10], [14]. Hensley *et al.* [22] compared repeat-pass polarimetric-interferometric data generated from UAVSAR flights with *in situ* M_v measurements to analyze the correlation between ΔM_v and φ. Their results showed that the interferometric correlation, either for the HH or VV polarizations, decreases as a function of increasing M_v differences between the observations. Moreover, Barrett *et al.* [12] used the DInSAR method to estimate ΔM_v over agricultural fields. Their results showed the correlation coefficients (r) varying between 0.51 and 0.81, depending on crop types. Moreover, it was observed that the C-band cross-polarization pairs provided the highest r values over the barley and potato fields with $r = 0.51$ and $r = 0.81$, respectively. In another study, De Zan *et al.* [8] proposed a model based on plane waves to model the vertical complex wavenumbers in the soil as a function of geometrical and dielectric properties and the complex interferometric coherences using L-band airborne SAR data. Additionally, Zwieback *et al.* [10] used airborne L-band data to investigate the correlation between ΔM_v and φ, γ, and Ξ using regression techniques. Their results showed that φ was more sensitive to M_v compared to the other two indicators. The

Manuscript received March 3, 2021; revised April 27, 2021 and June 18, 2021; accepted July 6, 2021. Date of publication July 9, 2021; date of current version July 28, 2021. *(Corresponding author: Sadegh Ranjbar; Meisam Amani.)*

Sadegh Ranjbar and Mehdi Akhoondzadeh are with the School of Surveying and Geospatial Engineering, College of Engineering, University of Tehran, Tehran 14398143141, Iran (e-mail: s.ranjbar72@ut.ac.ir; makhonz@ut.ac.ir).

Brian Brisco is with the Canada Center for Mapping and Earth Observation, Ottawa, ON K1S 5K2, Canada (e-mail: brian.brisco@canada.ca).

Meisam Amani is with Wood Environment & Infrastructure Solutions, Ottawa, ON K2E 7L5, Canada (e-mail: meisam.amani@woodplc.com).

Mehdi Hosseini is with the Department of Geographical Sciences, University of Maryland, College Park, MD 20742 USA (e-mail: mhoseini@umd.ed).

Digital Object Identifier 10.1109/JSTARS.2021.3096063

highest sensitivity derived at the HH polarization. Zwieback *et al.* [14] also analyzed whether M_v can be estimated from the three DInSAR observations with the purpose of separating M_v and effects of displacements on φ. They estimated M_v from the three DInSAR observables including φ, γ, and Ξ without making any assumptions about M_v complex spatiotemporal dynamics. Their results showed M_v time series up to an overall offset can be estimated using φ. They concluded that separating displacements and ΔM_v was challeging using only DInSAR observations. De Zan *et al.* [9] also used ALOS-2/PALSAR-2 L-band images to retrieve M_v from SAR Ξ. They showed that there were ambiguities to estimate M_v using only Ξ. They used γ to solve the ambiguities effect. Their results illustrated that there was a high degree of correlation between 50 and 75%. Furthermore, Molan *et al.* [9] studied the possibility of the ΔM_v estimation using γ and Ξ in the semisynthetic multi-looked interferograms. Their results showed Ξ and decorrelation were increased with increasing ΔM_v. Additionally, their results showed that the variations of φ, γ, and Ξ were associated with land cover type. Overall, their results illustrated γ and Ξ were unsuitable for estimating ΔM_v [23].

None of the previous studies has investigated the potential of φ to estimate ΔM_v in C-band. Moreover, the suitability of φ for estimating ΔM_v depends on multiple factors, such as land cover, but these dependencies have not been thoroughly studied, especially using C-band data. Additionally, the relationship between φ and ΔM_v at different crop growth stages has not been investigated in previous studies. Therefore, this study's aims are itemized in the following: 1) Investigation of the potential of φ in C-band data for ΔM_v estimation over wheat, canola, corn, soybean, and bare fields using linear regression models, 2) comparing the potential of φ in C-band for ΔM_v estimation with the potential of φ in L-band. The main focus of this study was on C-band results; however, L-band was also assessed to investigate wavelength effects. To this end, Sentinel-1 (C-band) and airborne UAVSAR (L-band) data over two study areas in Canada were employed. The small spatial and short ΔT are expected to reduce the impacts of the other potential factors (e.g., deformation, atmosphere, and topography). Furthermore, as the sensitivities of different polarizations to M_v are not necessarily identical, the sensitivity analysis was also performed for different polarizations.

II. Radar Interferometry

The φ is the phase difference between the two single look complex (SLC) images. In a radar system with a quad-polarization framework [24], each SLC pixel corresponds to a scattering matrix S

$$S = \begin{bmatrix} S_{HH} & S_{HV} \\ S_{VH} & S_{VV} \end{bmatrix} \tag{1}$$

where S_{jk} is the backscatter from *j* receiving and *k* transmitting polarizations.

Each SLC pixel can also be described by a scattering vector q; in the lexicographic basis (reciprocal backscatter situation), $q = [\, S_{HH}\ S_{HV}\ S_{VV}\,]^T$. In a polarimetric framework, if q_m and q_n are two scattering vectors of two SLC images, the interferometric signal can be represented by the covariance matrix $C_{n,m} = \langle q_n\ q_m^{\dagger}, \rangle$ where † denotes conjugate transpose and the $\langle \cdot \rangle$ denotes an ensemble average, which can be estimated by spatial multilooking [25], [26] of acquisitions *m* and *n*

$$\gamma_{n,m}\ (\omega) = \frac{\omega^{\dagger} C_{n,m}\omega}{\sqrt{(\omega^{\dagger} C_{n,n}\omega)(\omega^{\dagger} C_{m,m}\omega)}} = |\gamma_{n,m}\ (\omega)|\ e^{j\varphi_{n,m}(\omega)} \tag{2}$$

where coherence magnitude $|\gamma|$ and φ are the magnitude and argument of the complex correlation coefficient $\gamma_{n,m}$ for a specified polarimetric projection vector ω, respectively [24]. ω is a polarimetric unitary projection vectors (e.g., $\omega = [0\ 0\ 1]^T$ for VV).

The φ parameter can be decomposed into multiple contributions. The phase of the received signal is not only determined by only the effects of ΔM_v and vegetation changes (ΔV) but also other factors, including deformations, wind speed/direction, atmospheric conditions, and the topography are effective. Short spatiotemporal baselines are preferred in practice to diminish the additional influences, such as deformation and the topography. After removing the flat earth and topographic phase components, the φ can be decomposed as follows [10], [15], [27]:

$$\begin{aligned} \varphi_{\text{DInSAR}} = \varphi_{\text{def}} + \varphi_{\text{soil}} + \varphi_{\text{veg}} + \varphi_{\text{topo\_res}} \\ + \varphi_{\text{atm\_d}} + \varphi_{\text{orb\_d}} + \varphi_{\text{noise}}. \end{aligned} \tag{3}$$

In which φ_{def} models the phase term associated with the surface deformation [28], [29]. φ_{soil} is the phase changes due to the surface changes [30]. φ_{veg} is the phase changes due to the vegetation changes [31]. $\varphi_{\text{topo\_res}}$ is the residual topographic error (RTE) component. $\varphi_{\text{atm\_d}}$ is the difference of the atmospheric impacts for the two acquisitions. $\varphi_{\text{orb\_d}}$ is the difference of the phase component due to the difference of the orbital errors of each image. φ_{noise} models the phase component associated with the noises.

III. Study Areas and Dataset

In this article, Sentinel-1A (C-band) data along with soil moisture active passive validation experiment 2016 Manitoba (SMAPVEX16-MB) [32] ground measurements, as well as airborne UAVSAR (L-band) data along with Canadian Experiment for Soil Moisture in 2010 (CanEx-SM10) [33] ground measurements were used. The corresponding study areas and datasets are explained and compared in the following three subsections.

A. SMAPVEX16-MB Campaign and Sentinel-1 (C-Band) Data

The SMAPVEX16-MB campaign was conducted near Winnipeg, Manitoba (MB), Canada, with an area of 26 by 48 km (latitude = 49.3°N to 49.8°N and longitude = 97.7°W to 98.2°W) [see Fig. 1(a)]. During the SMAPVEX16-MB campaign, *in situ* measurements of soil and vegetation characteristics were collected over 50 agricultural fields to support calibration and validation of the soil moisture active passive (SMAP) satellite mission [32]. Table II presents the average meteorological conditions and M_v at ground measurement stations at the time of image acquisitions. Wheat, winter wheat, canola, corn, soybeans,

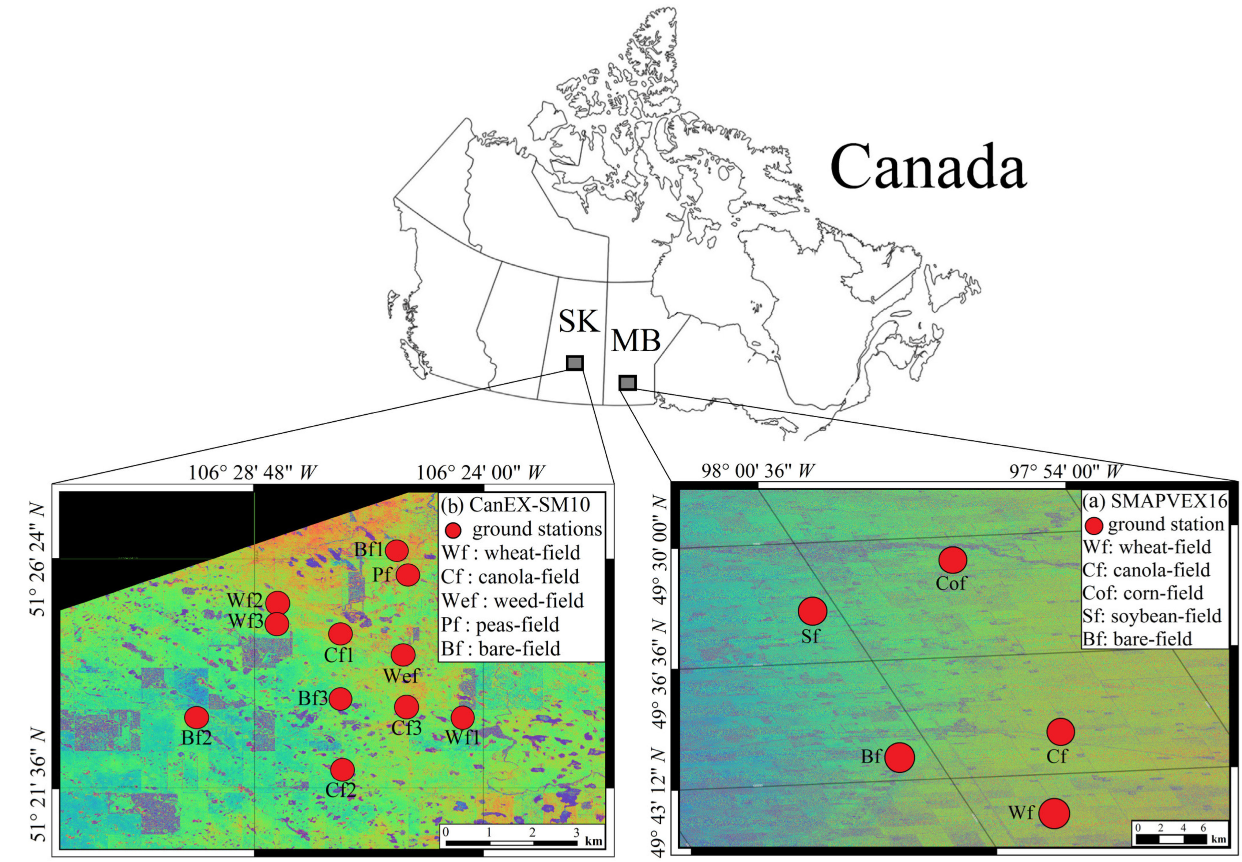

Fig. 1. Locations of the two study areas in Canada and the distributions of the sampling points on: (a) an interferogram between DOY 154 and DOY 166 of the SMAPVEX16-MB campaign, and (b) an interferogram between DOY 156 and DOY 159 of the CanExSM10 campaign.

and oats are the major crops grown in this area [32]. M_v were mainly measured at the soil depth of 5 cm, but it is also measured at the depths varying between 5 and 50 cm over the permanent stations. The M_v measurements at 0–5 cm were used in this study. *In situ* measurements from one of the fields of wheat, canola, corn, soybean, and bare were considered to investigate the objective of this study for different crop types. In this campaign, M_v measurements at 0–5 cm of soil, vegetation biomass change (Δb), and vegetation height change (Δh) were extracted and used for the analyses (see Section V). The sites which were used in this study are shown in Fig. 1(a). The temporal pattern of ΔM_v variability is consistent with $\varphi_{\mathrm{DInSAR}}$ variability. Fig. 2(a) shows the time series of ΔM_v, $\varphi_{\mathrm{DInSAR}}$,vegetation Δb, and vegetation Δh for three samples. All differences are from the master at DOY 191.

In total, 12 C-band Sentinel-1A single look complex (SLC) images were used in this article. These data were acquired between May 13 2016 and Aug 24 2016 in the Interferometric Wide swath (IW) mode, which are freely accessible from[1] (see Table I for more details). Sentinel-1A IW mode data provide SLC images with the 5 by 20 m spatial resolution at the VV and VH polarizations. IW mode acquired three subswaths using the terrain observation with progressive scans SAR (TOPSAR) with a swath width of 251.8 km [30]. The TOPSAR mode replaces the conventional ScanSAR mode, obtaining the same resolution and coverage as ScanSAR, but with a better signal-to-noise ratio and distributed target ambiguity ratio.

[1][Online]. Available: https://search.asf.alaska.edu.

B. CanEx-SM10 Campaign and UAVSAR (L-Band) Data

CanEx-SM10 campaign covers an area of approximately 45×70 km and is located in Kenaston, SK, Canada (51° 30' N, 106° 18' W) [see Fig. 1(b)]. L-band UAVSAR data were collected while measuring ground data during the CanEx-SM10 campaign. Measurements of vegetation properties and soil were accumulated from Jun 2, 2010 to Jun 14, 2010 during this campaign to support algorithm development, validation, and calibration processes of the soil moisture ocean salinity (SMOS) and SMAP satellite missions [33]. The area is covered by grassland, pastures, and rainfed agricultural fields. M_v was measured hourly at the permanent stations at several soil depths, and over twenty fields using the Stevens hydraprobe sensors [10], [33].

In situ measurements of vegetation characteristics [i.e., vegetation height (h), leaf area index (LAI), biomass (b)] and soil [i.e., temperature (T), moisture (M_v), bulk density, roughness (S)] were conducted over this study area. Widespread swelling and shrinking are not expected because the soil is mainly loamy [14], [33]. Remote sensing airborne and satellite data were acquired very close to the time of ground measurements [33]. We used the 0–5-cm soil moisture measurements. In this case study, we did our tests over five fields of wheat, canola, bare, weed, and peas. However, most of these fields were bare or partially covered with the harvest leftovers [33]. Since the temporal baselines (ΔT)

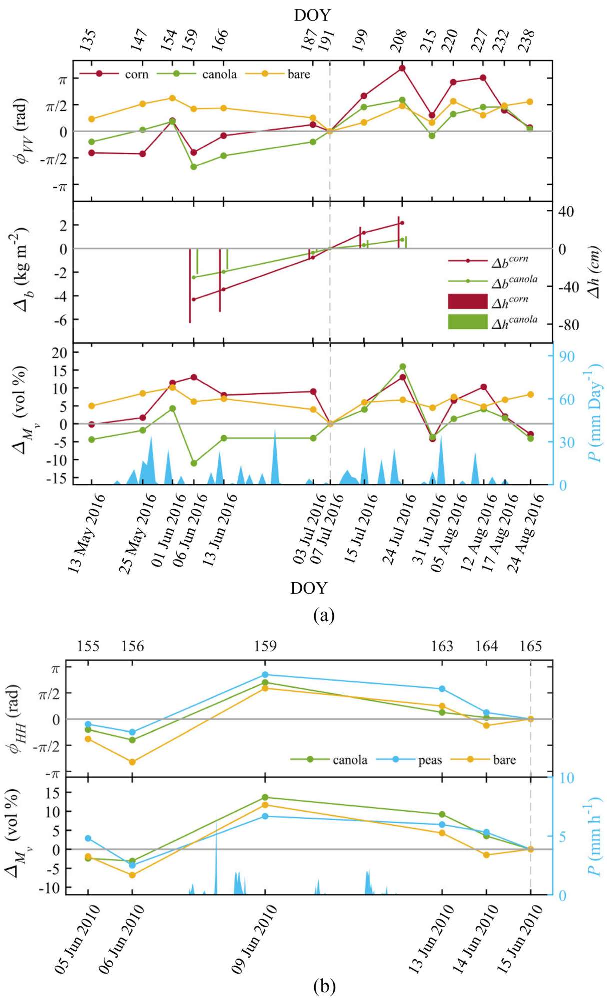

Fig. 2. (a) and (b) illustrate time series changes of DInSAR phase, soil moisture, and vegetation over the SMAPVEX16-MB and CanEx-SM10 campaigns, respectively. The blue bars denote the measured precipitation rate in bare fields.

are shorter than 11 days for the data collected for this campaign, the land cover change is negligible [10]. The meteorological conditions and range of the M_v at the time of image acquisitions are provided in Table I. During the data acquisition, soil surface measurements (e.g., T, M_v , S), vegetation properties (e.g., h, LAI, and b), and crop type were collected for most fields [33]. The locations of these measurements are shown in Fig. 1(b). The temporal pattern of ΔM_v variability is consistent with φ_{DInSAR} variability. Fig. 2(b) shows the temporal progress of ΔM_v and φ_{DInSAR} for three samples. The master was at DOY 165. The M_v measurements at the depth of 0–5 cm were used for the tests.

We used six L-band UAVSAR images at the approximately zero spatial baselines for the tests (see Table I). The UAVSAR data are quad-polarization (VV, VH, HH, and HV) and have a resolution of 0.8 and 1.7 m in the azimuth and range directions, respectively [34], [35]. UAVSAR, a Jet Propulsion Laboratory (JPL)-built reconfigurable, polarimetric L-band synthetic aperture radar (SAR), is specifically designed to obtain airborne repeat-track SAR data for differential interferometric measurements [33].

C. Comparison of the Two Field Campaigns

The main specifications of the two campaigns are listed in Table II. The major difference between the two campaigns is related to the data acquisitions which are in two radar frequencies, including high-frequency C-band and low-frequency L-band. This allows us to investigate the difference between short and long wavelengths in estimating ΔM_v under different vegetation conditions. Another obvious difference between the two field campaigns is the period for collecting field data. During the CanEx-SM10 campaign, the ΔT of the interferograms is much shorter than the ΔT of interferograms for the SMAPVEX16-MB. By examining the results of this difference, the effect of ΔT on the estimation of ΔM_v is evaluated. The different growth stages as a discrepancy of the two campaigns allowed us to investigate the plants' influences on ΔM_v estimation more precisely. The spatial resolution of the two sensors is another difference where the resolution of Sentinel-1A IW SLC data is 5×20 m, and the resolution of UAVSAR is 0.8 m in azimuth and 1.7 m in range.

IV. Assumptions

In order to reduce the complexity of (3), the phase components were divided into two subgroups of 1) nuisance components (i.e., $\varphi_{\text{topo\_res}}$, $\varphi_{\text{atm\_d}}$, $\varphi_{\text{orb\_d}}$, and φ_{noise}), which were not considered in the analysis, and 2) considered components (i.e., φ_{soil} and φ_{veg}), which were considered in the analysis. The reason is the effects of nuisance components are very small and negligible compared to the impacts of ΔM_v and ΔV on φ due to the small spatiotemporal baselines of the data used in this study. Therefore, the error of removing them with existing methods reduces the correlation between ΔM_v and φ. By the above explanations, the following subsections elaborate on the assumption, which were considered to minimize the magnitude of these nuisance components and to prevent decreasing the correlation between ΔM_v and φ.

A. Nuisance Components

According to the short spatiotemporal baselines, φ_{def}, $\varphi_{\text{topo\_res}}$, $\varphi_{\text{atm\_d}}$, $\varphi_{\text{orb\_d}}$, and φ_{noise} in (3) were not considered in the calculation. This is because the magnitudes of these components are negligible compared to ΔM_v and ΔV in short spatiotemporal baselines ($\Delta\text{T} < 12$ days, perpendicular baseline difference (PBD) < 150 m) [10], [14]. After removing the $\varphi_{\text{atm\_d}}$ and $\varphi_{\text{orb\_d}}$ or reducing the φ_{noise} using spatial filtering, the correlation between φ_{DInSAR} and ΔM_v is reduced. This means that removing these components adds additional errors that affect the correlation between φ_{DInSAR} and ΔM_v more than the magnitude of nuisance components. Therefore, the elimination of these components was not considered in this research. However, a method based on two variable normal distribution of φ_{DInSAR} and ΔM_v was considered to eliminate the contributions of nuisance components in ΔM_v estimation by removing abnormal data (see Section V-C). Moreover, since ΔT is shorter than 11 days for all the pairs in the CanEx-SM10 campaign and shorter than 25 days for most of the pairs in the

TABLE I
DATES OF SATELLITE IMAGES ACQUISITIONS AND METEOROLOGICAL CONDITIONS AT THE TIME OF THE ACQUISITIONS

Data	Date (d m y)	IA_{CS} (degree) [near–far]	3-days P (mm) [min-max]	AM_v (vol. %) [min-max]	Wind (knots) [Ws, Wd]	Temp. (◦C) [Air, Soil]
Sentinel-1A	13 May 2016	[35.98-41.70]	[0-0]	[15.2-38.5]	[4.990, 322.4]	[03.7, 05.7]
	25 May 2016	[36.20-41.64]	[30.2-38.14]	[17.1-39.4]	[2.172, 92.50]	[15.1, 14.8]
	01 Jun 2016	[30.56-36.37]	[22.6-29.3]	[26.8-44.9]	[4.657, 71.98]	[12.4, 13.6]
	06 Jun 2016	[36.20-41.64]	[0.9-7.4]	[19.7-42.3]	[7.695, 321.5]	[13.5, 14.1]
	13 Jun 2016	[30.30-36.53]	[23.8-27.6]	[24.8-40.9]	[0.732, 172.5]	[12.5, 13.8]
	03 Jul 2016	[33.10-39.65]	[1.3-8.60]	[13.4-33.1]	[1.500, 83.49]	[14.5, 16.2]
	07 Jul 2016	[30.30-36.53]	[0 -0]	[15.4-38.1]	[0.018, 17.49]	[15.3, 18.1]
	15 Jul 2016	[33.10-39.65]	[16.3-26.60]	[27.1-43.4]	[2.300, 155.9]	[17.4, 18.]
	24 Jul 2016	[35.98-41.72]	[24.8-31.1]	[28.7-42.8]	[2.327, 248.9]	[18.2, 19.1]
	31 Jul 2016	[30.30-36.53]	[7.1-9.6]	[11.2-42.7]	[1.101, 145.0]	[19.1, 20.7]
	05 Aug 2016	[35.98-41.70]	[32.3-37.4]	[21.9-41.3]	[1.136, 270.8]	[16.0, 17.0]
	12 Aug 2016	[30.30-36.53]	[19.80-26.0]	[25.7-39.4]	[0.303, 280.0]	[16.5, 19.0]
	17 Aug 2016	[35.98-41.85]	[4.30-10.2]	[17.4-41.2]	[0.394, 236.4]	[16.1, 18.9]
	24 Aug 2016	[30.30-36.53]	[0.02-0.7]	[12.5-38.9]	[1.354, 291.4]	[17.4, 19.2]
UAVSAR	05 Jun 2010	[36.43-47.86]	0	[28.4-38.4]	[-,-]	[-, 13.7]
	06 Jun 2010	[36.43-47.86]	0	[27.5-38.0]	[-,-]	[-, 14.2]
	09 Jun 2010	[36.43-47.86]	19.4	[29.0-38.0]	[-,-]	[-, 12.8]
	13 Jun 2010	[36.43-47.86]	17.6	[32.3-41.0]	[-,-]	[-, 11.9]
	14 Jun 2010	[36.43-47.86]	6.3	[30.1-39.5]	[-,-]	[-, 11.2]
	15 Jun 2010	[36.43-47.86]	0	[31.5-39.8]	[-,-]	[-, 11.3]

IA_{CS} = Incidence angle over the study area, AM_v = average volumetric soil moisture, 3-days P = average accumulative three-day precipitation at the stations, Ws = average wind speed at the stations, Wd = average wind direction at stations, Air = average air temperature and Soil = average 0-5 cm soil temperature.

TABLE II
COMPARISON OF THE TWO FIELD CAMPAIGNS

	SMAPVEX16-MB campaign (Sentinel-1A IW)	**CanEx-SM10 campaign (UAVSAR)**
Mission duration	May 1 to Aug 31, 2016	Jun 1 to Jun 17, 2010
Land cover types	wheat, canola, corn, soybean, and bare	wheat, canola, weeds, peas, and bare
Centre frequency	C-Band 5.405 GHz (a wavelength of 5.546 cm)	L-Band 1257.5 MHz (a wavelength of 23.85 cm)
Altitude	693 km	13 km
Repeat cycle	12 days	-
Polarization	VV and VH	Full Quad-Polarization
Incidence angle	$20^{\circ}-46^{\circ}$	$25^{\circ}-65^{\circ}$
Bandwidth	56 MHz (0-100 MHz programmable)	80 MHz
Spatial resolution	$5\,m \times 20\,m$	0.8 m in Azimuth and 1.7 m in Range

SMAPVEX16-MB campaign, φ_{def} was considered negligible. $\varphi_{\mathrm{DInSAR}}$ for pairs in CanEx-SM10 campaign does not have $\varphi_{\mathrm{topo\_res}}$ due to zero spatial baseline, and $\varphi_{\mathrm{topo\_res}}$ has also been considered negligible for SMAPVEX16-MB campaign, as this component magnitude is negligible compared to ΔM_v and ΔV contribution.

B. Considered Components

Due to the significant effects of the two components of ΔM_v and ΔV, especially in C-band, these two components are used in the development of the linear model in this article. More penetration of L-band in the vegetation causes slight vegetation changes to have less effect on the radar signal in L-band than the C-band. Therefore, modeling M_v variations is more accurate at L-band during the crop growing season [14], [36], [37].

1) Phase $\boldsymbol{\varphi_{\mathrm{soil}}}$*:* Four hypotheses, explained by [10], describe the physical process underlying φ_{soil}, which are taken from the origins of the M_v effects on received signal. Null (no relationship between φ_{soil} and M_v), wetting/drying cycle impacts on swelling soil behavior, penetration depth of signal, and dielectric impacts on the signal are the four hypotheses. The physical processes of hypotheses are not necessarily mutually exclusive. However, in this article, the modeling between ΔM_v and φ was established by a linear regression model described in regression model and estimation subsection because the linear regression model has provided appropriate results with acceptable accuracy in [10], [14], and [31].

2) Phase φ*_veg:* The impacts of vegetation canopy on the electromagnetic scattering have been studied in [31], [42], and [43]. φ between two acquisitions which is derived in vegetation growth steps can be significantly affected depending on the sensor frequency [31], [43]. For example, the vegetation growth in the initial and final steps are invisible in low-frequency data (e.g., L-band) [31], [43]. Due to many unknown effects of plant changes on the interferometric signal in C-band (high frequency), advanced modeling of the effect of vegetation changes on the φ was avoided because of avoiding further complexity. According to the objective of this article, the modeling between φ and ΔM_v was established using a linear model (see Section V-E1) to investigate the suitability of using φ for ΔM_v estimation in C-band over different land covers. However, φ_veg was not considered in the CanEx-SM10 campaign because L-band data is used in this campaign and the invisibility of small vegetation changes due to very short ΔT (i.e., <11 days).

TABLE III
CHARACTERISTICS OF SENTINEL-1A AND UAVSAR DINSAR PAIRS

	no.	MID	SID	ΔT	PBD	DCD
Sentinel-1A IW SLC pairs in SMAPVEX16-MB	1	13 May	25 May	12	126	3.71
	2	13 May	06 Jun	24	135	-4.63
	3	13 May	24 Jul	72	73	0.72
	4	13 May	05 Aug	84	118	3.93
	5	13 May	17 Aug	96	60	-2.9
	6	25 May	06 Jun	12	6	8.33
	7	25 May	24 Jul	60	27	3.67
	8	25 May	05 Aug	72	72	0.64
	9	25 May	17 Aug	84	12	-3.78
	10	06 Jun	24 Jul	48	21	4.37
	11	06 Jun	05 Aug	60	110	8.28
	12	06 Jun	17 Aug	72	81	6.46
	13	24 Jul	05 Aug	12	6	7.91
	14	24 Jul	17 Aug	24	6	2.67
	15	05 Aug	17 Aug	12	8	5.24
	16	01 Jun	07 Jul	36	15	6.48
	17	01 Jun	13 Jun	12	9	8.91
	18	01 Jun	31 Jul	60	117	-1.96
	19	01 Jun	12 Aug	72	52	7.75
	20	01 Jun	24 Aug	84	8	-2.75
	21	07 Jul	13 Jun	24	76	1.74
	22	07 Jul	31 Jul	24	6	-0.09
	23	07 Jul	12 Aug	36	53	1.97
	24	07 Jul	24 Aug	48	84	-2.55
	25	13 Jun	31 Jul	48	71	-1.66
	26	13 Jun	12 Aug	60	55	-3.76
	27	13 Jun	24 Aug	72	82	2.11
	28	31 Jul	12 Aug	12	47	-2.06
	29	31 Jul	24 Aug	24	17	1.96
	30	12 Aug	24 Aug	12	47	-0.26
	31	03 Jul	15 Jul	12	21	+1.07
UAVSAR pairs in CanEx-SM10	1	05 Jun	06 Jun	1	0	3.07
	2	05 Jun	09 Jun	4	0	-0.76
	3	05 Jun	13 Jun	8	0	0.32
	4	05 Jun	14 Jun	9	0	0.74
	5	05 Jun	15 Jun	10	0	-0.28
	6	06 Jun	09 Jun	3	0	3.18
	7	06 Jun	13 Jun	7	0	-2.43
	8	06 Jun	14 Jun	8	0	-3.91
	9	06 Jun	15 Jun	9	0	0.09
	10	09 Jun	13 Jun	4	0	3.31
	11	09 Jun	14 Jun	5	0	0.02
	12	09 Jun	15 Jun	6	0	-0.51
	13	13 Jun	14 Jun	1	0	-0.61
	14	13 Jun	15 Jun	2	0	1.1

MID = Master image date, SID = Slave image date, ΔT = Temporal baseline, PBD = Perpendicular baseline difference (m), T/f = Track/frame, DCD= Doppler Centroid Difference (Hz).

V. DATA ANALYSIS

A. SAR Data Processing

For the SMAPVEX16-MB campaign, we tried to form interferograms between pairs with perpendicular baseline difference less than 150 m [12], [21], which resulted in a total of 31 interferograms (see Table III). In order to generate interferograms of this campaign, the InSAR pairs were coregistered using the S1-TOPS coregistration module in S1-toolbox [38]. Coregistration accuracy can be reached at a 1/100 azimuth pixel level by applying the cross-correlation matching procedure. Then, $|\gamma|$ and φ were produced for the InSAR pairs using S1-toolbox [38]. Subsequently, the flat earth and topographic phase correction was applied to the interferograms of the SMAPVEX16-MB campaign. Finally, to prepare products for analysis, a filter adaptively applied to the products to reduce noise effects.

In the CanEx-SM10 campaign, we estimated covariance matrices $C_{n,m}$ between acquisitions n and m by combining the radar data interferometrically [24]. The raw interferograms had an unknown phase offset and trends. The offset was referenced using a nearby persistent scatterer for each field separately; see [10] to analyze the sensitivity with respect to the referencing. However, the data contain kilometre-scale residual phase contributions because of the atmosphere and orbital errors, which we do not attempt to eliminate. In this campaign, the complex interferograms were formed for all the possible image pairs from the CanEx-SM10 campaign, resulting in 15 interferograms (see Table III). In the CanEx-SM10 campaign, the flat earth and topographic phase correction was not necessary because of the zero spatial baselines between the InSAR pairs.

According to Table III, the perpendicular baselines of the DInSAR pairs for the CanEx-SM10 campaign are zero and for the SMAPVEX16-MB campaign are from 6 to 135 m. The DInSAR pairs for the CanEx-SM10 campaign had ΔT from 1 to 10 days and for the SMAPVEX16-MB campaign, they are between 12 and 96 days. These pairs were selected based on to have: 1) The Doppler centroid difference below $\sim$10 Hz to minimize the decorrelation; 2) the spatial baselines as small as possible. For example, the pairs with perpendicular baselines less than 150 m for the SMAPVEX16-MB campaign were selected, and the pairs had approximately zero perpendicular baselines for the CanEx-SM10 campaign; and 3) ΔT less than 100 days for the SMAPVEX16-MB campaign, and less than 10 days for the CanEx-SM10 campaign.

B. In Situ Data Processing

After generating interferograms and applying the flat earth and topographic phase correction to the SMAPVEX16-MB interferograms, the φ associated with the ground measurement sites were extracted and used for the analysis. In the analysis process, the noisy data were omitted using a statistical filter. A statistical filter based on two variables normal distribution is considered to eliminate the contributions of nuisance components by removing noisy data [39], [40]. The decisions for normality at $\alpha = 0.05$ and the 95% confidence intervals were considered to remove noisy samples in all analyses, such as scattering plots, model estimation and its assessment process, as well as ΔM_v estimation. For instance, the scatter-plots between φ and ΔM_v along with their two-variables normal distribution are shown in Fig. 3. This indicates that the green scatters are used as normal data in analyses and the red ones were recognized as noisy data and were removed.

C. Visual Analysis

The scatter-plots of φ and ΔM_v were generated for different polarizations and crop types for visual analysis of the relationship (see Section VI-A). Additionally, a quantitative analysis of the γ for the two study areas was performed to determine the impacts of crop types, ΔM_v and ΔT (see Section VI-B). This quantitative analysis of γ was performed to investigate

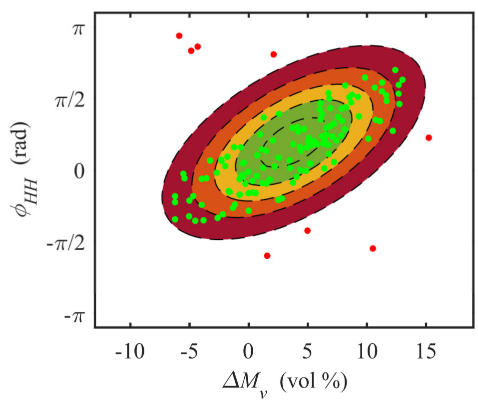

Fig. 3. Scatter-plots between φ and ΔM_v along with their two-variable normal distribution.

the source of errors in more details. By comparison between changes in φ and γ associated with ΔM_v, the source of errors was determined. For instance, a lack of correlation between ΔM_v and both γ and φ showed that the error is not based on deformation as γ is not affected by deformation. However, the source of reducing the correlation between ΔM_v and φ is highly due to deformation if the correlation between ΔM_v and γ is high and between ΔM_v and φ is low. Furthermore, this quantitative analysis is significantly affected by the difference in wavelength of the two campaigns, as the penetration of the L-band (~23 cm) is greater in the vegetation cover and, consequently, maintains higher coherence than the C-band (~5.6 cm).

D. Regression Model and Estimation

The relationship between ΔM_v and φ is established by a linear regression model. It was assumed that φ could be modeled by a simple regression model as a function of ΔM_v, and vegetation change (ΔV) in short spatiotemporal baselines, especially for significant changes of ΔM_v [10], [14]. The wet biomass (b) and crop height (h) measured during the SMAPVEX16-MB campaign were considered as vegetation descriptor. During this campaign, crops were fully developed and, thus, ΔV is significant. Therefore, both terms of ΔM_v and ΔV were used in the regression model to model φ. However, during the CanEx-SM10 campaign, most of the fields were bare or partly covered with harvest residues [33]. Therefore, the vegetation term was removed in the model for the CanEx-SM10 campaign. due to the very short ΔT, the vegetation changes were negligible for the fields covered with vegetation, and long wavelength (L-band) data [31], [41].

1) Regression Model: Equation (4) that was presented by [10] is the regression model that we have used in this article to describe the φ

$$\varphi_{ij} = \beta_{\Delta M_v} \Delta M_v + \beta_{\Delta V} \Delta V + \epsilon_{ij} \tag{4}$$

where the coefficient $\beta_{\Delta M_v}$ denotes the ΔM_v impacts on the φ. The effects of the ΔV is represented by the coefficient $\beta_{\Delta V}$. ϵ denotes the error term of the *i*, *j* interferogram.

2) Estimating the Regression Parameters: The regression parameters were computed using 60% of the ground measurements which were selected randomly for both case studies. The rest of the dataset (40%) was used to evaluate the performance of the model. The generalized least square (GLS) method [42] was applied for estimation of the model parameters (i.e., $\beta_{\Delta M_v}$ and $\beta_{\Delta \mathrm{V}}$). In this process, regression errors require a covariance matrix [10], which was modeled similar to [29]. In the regulation process, the statistical filter was used to reduce the effect of noise.

We used different sets of explanatory variables. For the SMAPVEX16-MB campaign, two configurations were considered for the estimation process.

Configuration 1: The vegetation wet biomass changes (Δb) and ΔM_v were used in the model regulation [see (4)].

Configuration 2: The vegetation height changes (Δh) and ΔM_v were used in the model regulation [see (4)].

The dates for the data (ΔM_v and φ) in bare fields were selected to be consistent with the date that vegetation data were collected in both configurations. Because, the same conditions (like weather) make a more reliable situation to analyze and compare results between the fields with vegetation cover and bare field.

For the CanEx-SM10 campaign, the vegetation term was not considered in the estimation process and only one configuration with ΔM_v was used in the estimation process.

E. Accuracy Assessment

In order to evaluate the model, 40% of the ground measurements, which were not considered for the regression model parametrization, were exclusively used. The numbers of samples in each field are demonstrated in Figs. 4, 5,6, and 11. Like other studies [43], statistical metrics, including coefficient of determination (R^2), root mean square error (RMSE), bias, and standard deviation (StDv) were calculated for the accuracy assessments.

VI. Results and Discussions

A. Phase Analysis

The scatter-plots of ΔM_v and φ for different polarizations and different crop types with different ΔT values are shown in Figs. 4 and 7. A positive and approximately linear relationship is observed between ΔM_v and φ, which correspond well with the results of [10], [12], [14]. However, the results for vegetation fields, especially for the SMAPVEX16-MB campaign (Fig. 7), show a low correlation. For instance, the scatter plots are associated with the VV polarization in the peas field in the CanEx-SM10 campaign [Fig. 4(d)] and the ones are associated with the VV and VH polarizations in wheat fields in the SMAPVEX16-MB campaign [Fig. 7(a) and (f)] show a nonlinear relationship between ΔM_v and φ. Although the results of vegetation fields in the SMAPVEX16-MB campaign (Fig. 7) show less correlation between ΔM_v and φ, the results of ΔT shorter than 25 days [the green dots in Fig. 7(a)–(d) and (f)–(i)] show a high correlation.

From Figs. 4 and 7, it is observed that increasing the ΔT results in lower correlations. For example, lower distribution in

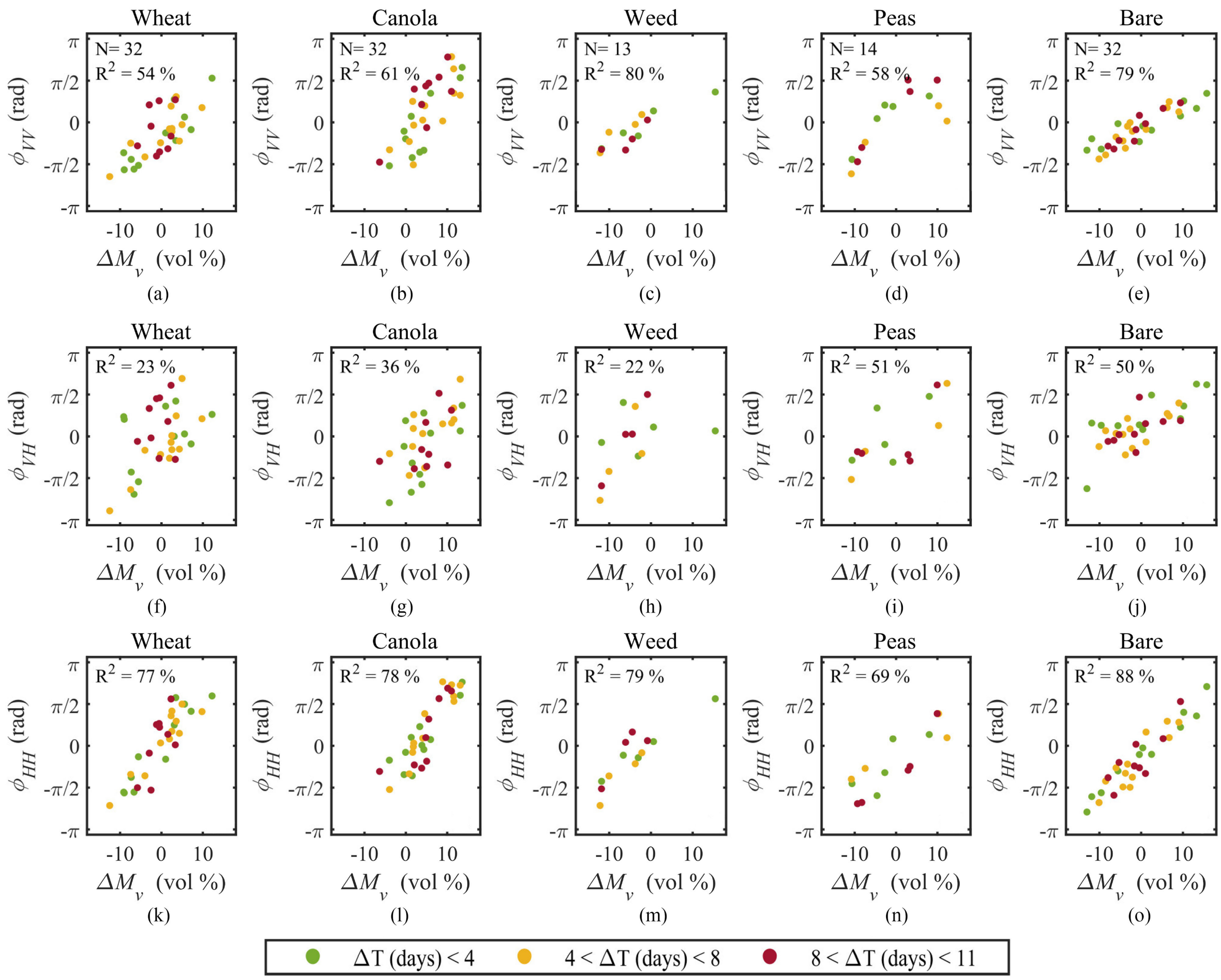

Fig. 4. Scatter-plots of φ and ΔM_v for the CanEx-SM10 campaign.

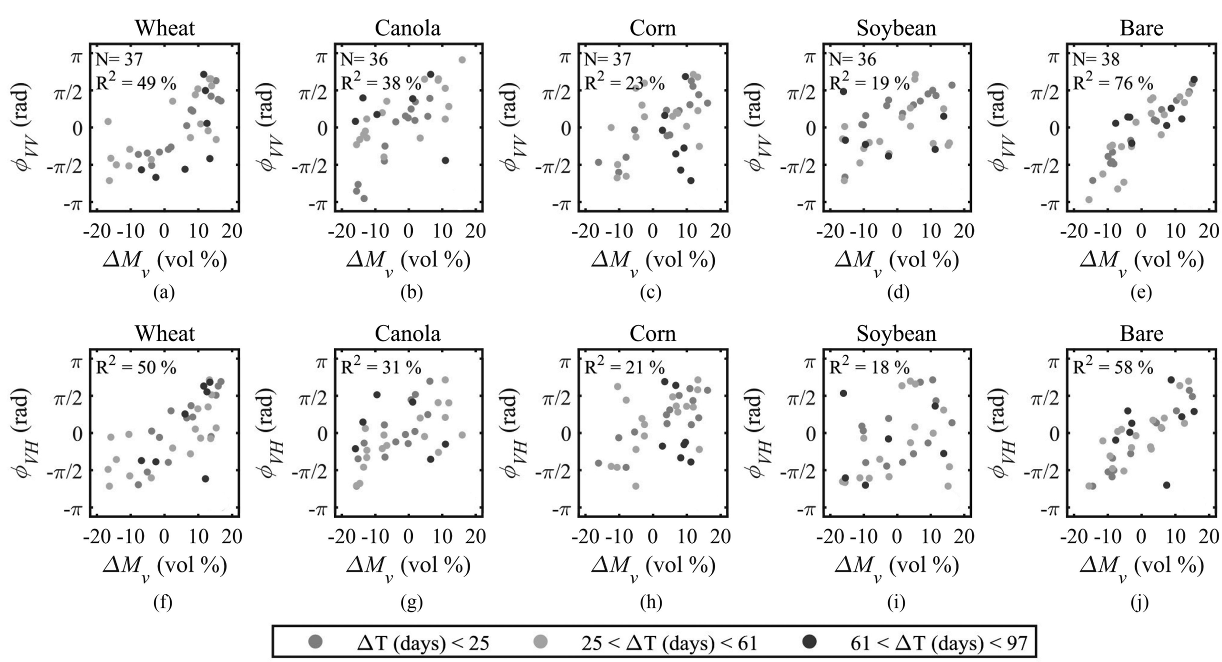

Fig. 5. Scatter-plots of γ and ΔM_v in CanEx-SM10 campaign.

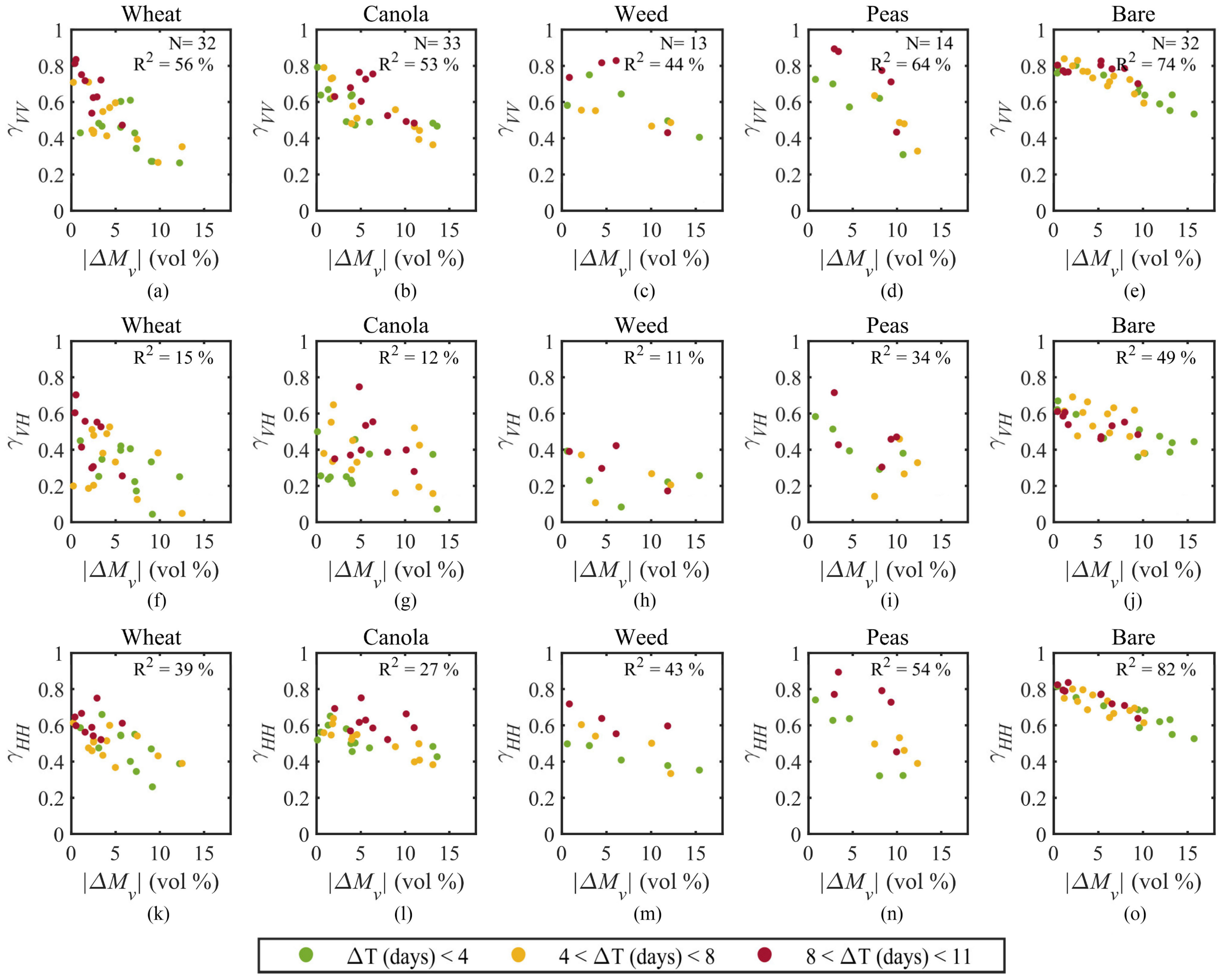

Fig. 6. Regression between the estimated and measured φ for the SMAPVEX16-MB campaign (a)-(j) for configuration 1 ($\beta_{\Delta M_v}$ and $\beta_{\Delta \mathrm{b}}$), and (k)-(t) for configuration 2 ($\beta_{\Delta M_v}$ *and* $\beta_{\Delta \mathrm{h}}$).

scatter-plots associated with the CanEx-SM10 is observed due to low differences between different ΔT (ΔT are shorter than 11 days). However, the effects of ΔT are significant for the SMAPVEX16-MB campaign, where ΔT values are between 12 and 96 days. This matter is discussed more in Section VI-G.

As it can be observed in Figs. 4 and 7, the highest correlation is obtained in the bare field, especially using the HH and VV polarizations with R^2 of 88% and 79%, respectively. According to Fig. 4, it can be observed that the higher distribution in scatters associated with the UAVSAR data is observed in the VH polarization for weed, wheat, and then canola with R^2 of 22%, 23%, and 36%, respectively. Despite bare field, weed shows the highest correlation in the VV and HH polarizations with R^2 of 80% and 79%, respectively. Regarding Sentinel-1 data, the plots show more distribution in scatters with R^2 of 19%, 23%, 38%, and 49% for soybean, corn, canola and wheat, respectively. In a comparison between different polarizations, it is observed that the copolarizations (HH and VV) show higher correlations than cross-polarization (VH) with R^2 of 55% to 80% depending on different crop fields in CanEx-SM10, and R^2 of 19% to 50% depending on different crop fields in SMAPVEX16-MB. By comparing the results from the two study areas, it is observed that the correlations are higher in the L-band (R^2 varies between 54% to 88%) compared to C-band (R^2 varies between 19% to 76%) depending on different fields. This is because, at a higher frequency (or shorter wavelength), the signal is highly affected by other factors, such as atmospheric condition, wind, and vegetation. Our results were similar to those of [9], [31].

B. Coherence Analysis

Figs. 5 and 8 show the observed relation between ΔM_v and γ for different crop types and different polarizations. The plots show a negative and approximately linear relationship between γ and ΔM_v which are similar to the results of the previous studies [18], [23]. Like the analysis of ΔM_v and φ scatters, noisy data was detected and was removed using the statistical filter in these results.

According to Fig. 8 (the plots associated with SMAPVEX16-MB campaign) and by comparing different ΔT values, it is observed that the γ significantly decreases by increasing ΔT. However, these results are not observed in the plots associated with the CanEx-SM10 campaign (Fig. 5), which could be due to the very short ΔT differences (i.e., shorter than 11

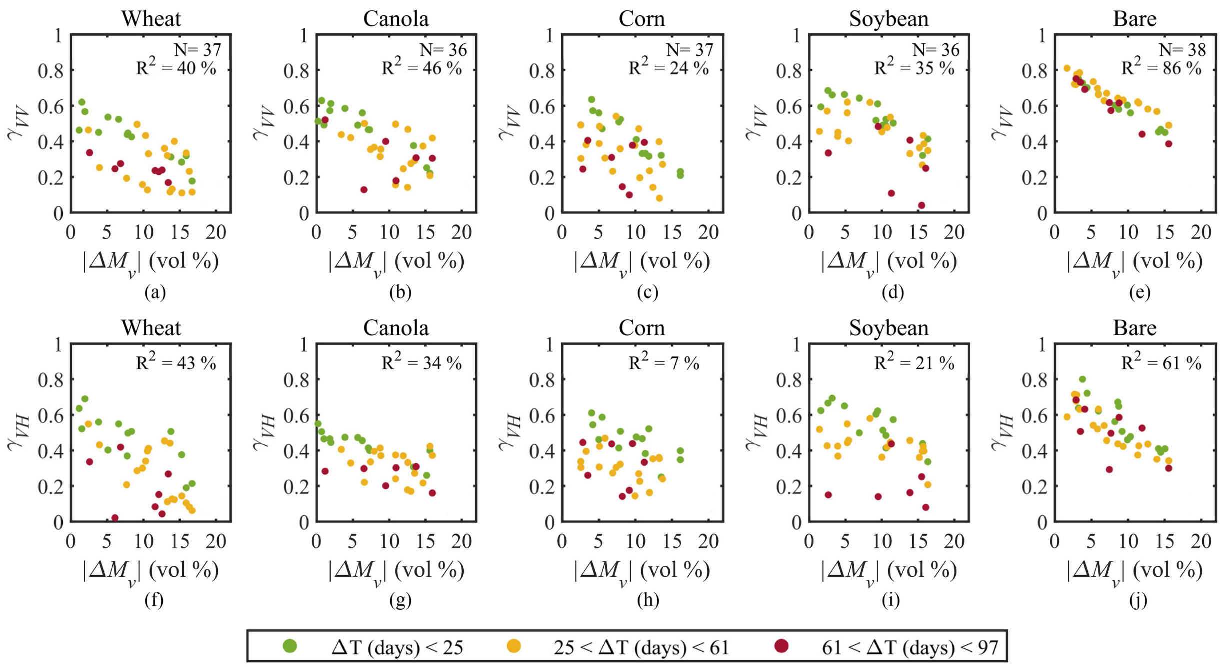

Fig. 7. Scatter-plots of φ and ΔM_v for the SMAPVEX16-MB campaign.

TABLE IV
Coherence Values for Different Crop Types, Temporal Baselines, and Polarizations

			wheat		**canola**		**corn**		**soybean**		**bare**	
			max	min	max	min	max	min	max	min	max	min
SMAPVEX16-MB	γ_{VV}	$\Delta T < 25$	0.62	0.18	0.63	0.22	0.63	0.21	0.68	0.32	0.75	0.45
		$25 < \Delta T < 61$	0.50	0.11	0.50	0.14	0.54	0.08	0.62	0.27	0.81	0.49
		$61 < \Delta T < 97$	0.34	0.17	0.52	0.13	0.40	0.10	0.48	0.04	0.75	0.39
	γ_{VH}	$\Delta T < 25$	0.69	0.19	0.55	0.26	0.61	0.25	0.69	0.34	0.80	0.39
		$25 < \Delta T < 61$	0.55	0.06	0.42	0.17	0.47	0.14	0.58	0.21	0.72	0.34
		$61 < \Delta T < 97$	0.42	0.02	0.31	0.16	0.44	0.14	0.44	0.08	0.68	0.29
			wheat		canola		weed		peas		bare	
			max	min	max	min	max	min	max	min	max	min
CanEx-SM10	γ_{VV}	$\Delta T < 4$	0.61	0.26	0.79	0.47	0.75	0.41	0.73	0.31	0.80	0.53
		$4 < \Delta T < 8$	0.71	0.27	0.79	0.36	0.56	0.47	0.64	0.33	0.84	0.59
		$8 < \Delta T < 11$	0.84	0.47	0.76	0.48	0.83	0.43	0.89	0.43	0.83	0.70
	γ_{VH}	$\Delta T < 4$	0.60	0.20	0.65	0.23	0.55	0.24	0.74	0.45	0.67	0.36
		$4 < \Delta T < 8$	0.63	0.15	0.75	0.26	0.47	0.21	0.56	0.24	0.69	0.38
		$8 < \Delta T < 11$	0.43	0.18	0.43	0.37	0.42	0.17	0.71	0.30	0.61	0.46
	γ_{HH}	$\Delta T < 4$	0.66	0.26	0.65	0.43	0.50	0.35	0.74	0.32	0.82	0.53
		$4 < \Delta T < 8$	0.61	0.37	0.64	0.38	0.60	0.33	0.53	0.39	0.80	0.61
		$8 < \Delta T < 11$	0.75	0.52	0.75	0.52	0.72	0.55	0.89	0.45	0.84	0.64

days). The correlations between ΔM_v and γ also decrease by increasing ΔT. These are more discussed in Section VI-G. Table IV presents the maximum and minimum of γ values for different ΔT, polarizations, and crop types. Comparing different γ values, bare field showed the higher and wheat showed the lower γ values in both campaigns (see Fig. 8 and Table IV). According to Fig. 8, the highest correlations between ΔM_v and γ in the SMAPVEX16-MB campaign were obtained in the VV polarization for bare, canola, and wheat with R^2 of 86%, 46%, 40%, respectively. Additionally, the lowest correlations were obtained in the VH polarization for corn and soybean with R^2 of 7% and 21%, respectively. According to Fig. 5, the highest correlations in the CanEx-SM10 campaign were also obtained in the VV and HH polarizations with R^2 of 39% to 82%, depending on different fields. Furthermore, the lowest correlations were obtained in the VH polarization for weed, canola, and wheat with R^2 of 11%, 12%, and 15%, respectively.

It is also observed that the scatters for the bare fields have higher γ and higher correlation. γ and φ behave similarly in different polarizations and it is observed that γ associated with co-polarization (γ_{VV} and γ_{HH}) have more correlation than cross-polarization (γ_{VH}). Therefore, according to γ and φ scattering results, it is concluded that the copolarization observations include more information for retrieving ΔM_v. According to

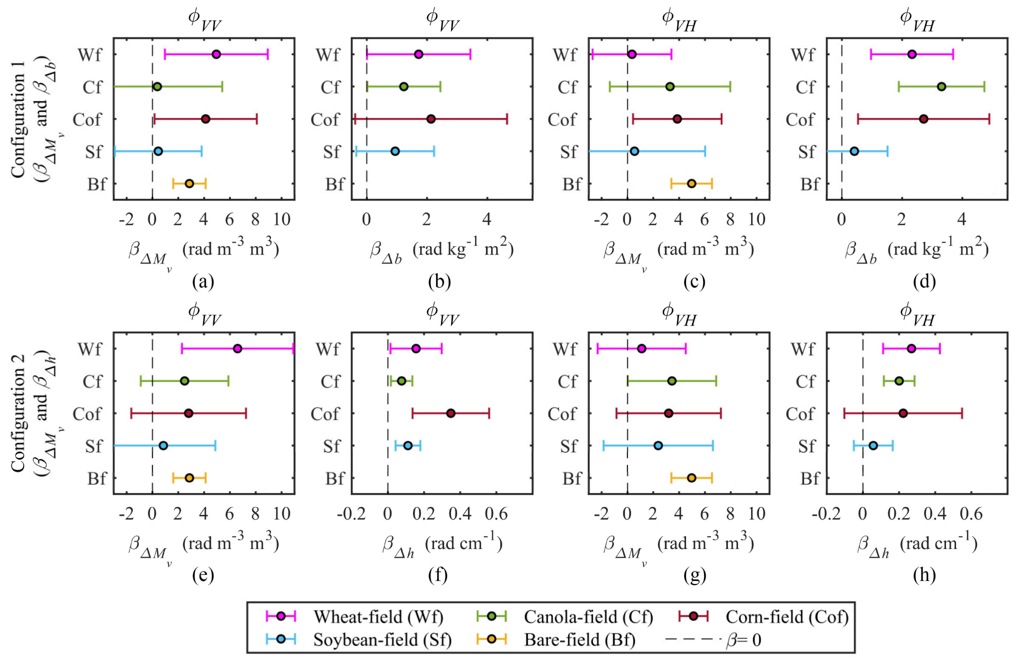

Fig. 8. Scatter-plots of γ and ΔM_v in SMAPVEX16-MB campaign.

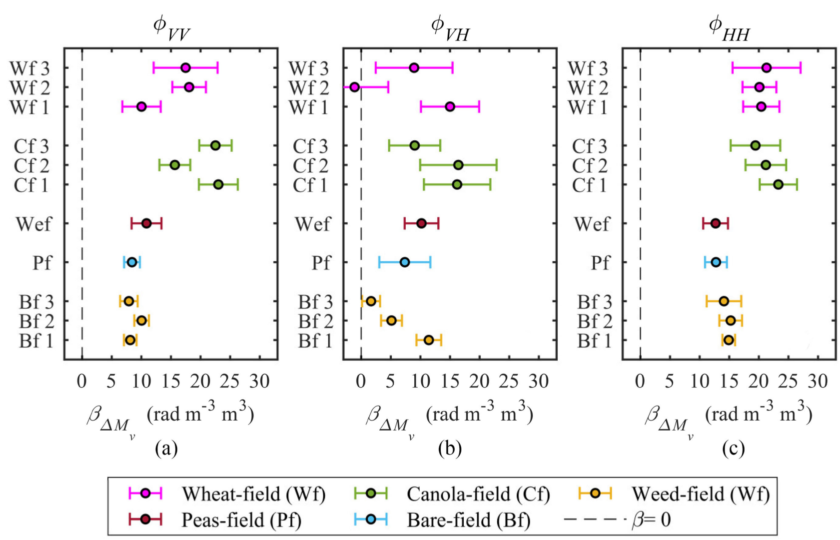

Fig. 9. Coefficients of the regression models [see (6)] in the SMAPVEX16-MB campaign. (a)–(d) show the coefficients of the configuration 1, and (e)–(h) show the coefficients of the configuration 2. The M_v coefficients are depicted in (a), (c), (e), and (g), and the vegetation descriptor coefficients are shown in (b), (d), (f), and (h).

Table IV, the difference between the lowest and highest values of γ in cultivated lands is very large. This indicates the effects of different vegetation conditions at the time of imaging on the γ are noticeable. Therefore, the scatter distribution of γ in crop fields is much higher than in the bare field. γ and φ in different polarizations behave similarly, for example, scatter-plots associated with VH are more dispersal. Comparing the two case studies in Figs. 5 and 8, it is observed that the γ for the CanEx-SM10 campaign (L-band) have higher correlations than those of the SMAPVEX16-MB campaign. This study observed that longer wavelengths (or lower frequencies) are less affected by plant growth. These results are consistent with previous studies (e.g., [12], [21]). For example, fewer correlations are observed in Figs. 5 and 8 over vegetated fields of the SMAPVEX16-MB campaign, which is related to C-band and its higher frequency which is highly affected by ΔV. It is worth noting that these results are well correspond to those of several studies such as [10] and [12].

C. Regression Model

1) Regression Model Estimation:: As described in Section V-E2, the regression model was adjusted using ΔM_v and φ. The estimated coefficients for the two configurations (e.g., configuration 1: $\beta_{\Delta M_v}$ and $\beta_{\Delta \mathrm{b}}$, and configuration 2: $\beta_{\Delta M_v}$ and $\beta_{\Delta \mathrm{h}}$) are depicted in Fig. 9(a)–(h) for the SMAPVEX16-MB campaign.

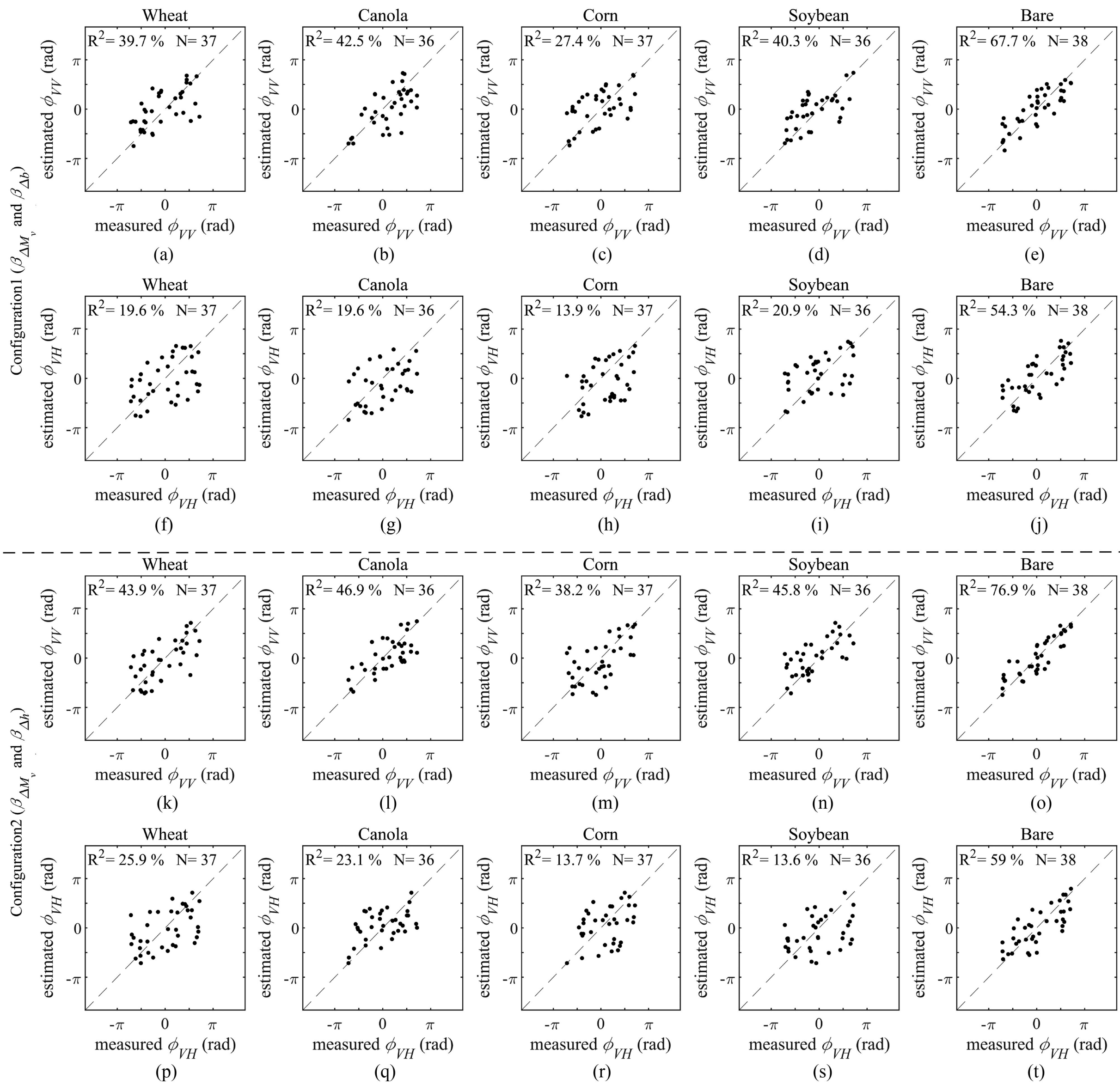

Fig. 10. M_v coefficients of the regression models for each field over the CanEx-SM10 campaign.

As shown in Fig. 9, all the obtained $\beta_{\Delta M_v}$ coefficients were positive, which indicates a positive relationship between φ and ΔM_v. The vegetation describer coefficients (i.e., $\beta_{\Delta \mathrm{b}}$ and $\beta_{\Delta \mathrm{h}}$) also indicate a positive relationship between φ and vegetation changes, indicating that an increase in plant growth makes an increase in φ and the $\beta_{\Delta M_v}$ coefficients. This can be observed in Fig. 3(a)–(h), in which the obtained $\beta_{\Delta M_v}$ coefficients in configuration 1 behave similarly to ones obtained in configuration 2 for different fields in both polarizations. However, due to varying types of data used for vegetation descriptor, the obtained $\beta_{\Delta V}$ coefficients show different behavior in the two configurations. The size of the effect of $\beta_{\Delta M_v}$ exceeds $2\ \mathrm{rad\ m^{-3} m^3}$ (i.e., an increase of 10 vol. % in M_v and a change of 11.4^{o} in φ) in 68% of the samples for the VV polarization and 54% of the samples for the VH polarization in configuration 1. These are also 76% of the samples in the VV polarization and 69% of the samples in the VH polarization in configuration 2.

For the CanEx-SM10 campaign, we estimated the M_v regression coefficients $\beta_{\Delta M_v}$ only when the vegetation term in (4) was considered negligible. This was explained in Section V-E2. The estimated $\beta_{\Delta M_v}$ coefficients for different crop types and different polarizations are plotted in Fig.10.

In this campaign, like SMAPVEX16-MB, all the coefficients are positive except for one of them in the VH polarization, which indicates a positive relationship between φ and ΔM_v. $\beta_{\Delta M_v}$ exceeds $5\ \mathrm{rad\ m^{-3} m^3}$ (i.e., an increase of 10 vol. % in M_v and a change of 28.6^{o} in φ) for 83%, 59%, and 78% of the samples in the HH, VH, and VV polarizations, respectively.

2) Accuracy Assessments: Statistical indices (e.g., R^2, RMSE, bias, and StDv) were used to evaluate estimation accuracy. The results are presented and discussed in the following subsections for the two study regions.

By comparing the estimated φ using the adjusted regression model and the obtained φ from the interferograms, the

TABLE V
ACCURACY OF THE MODEL REGULATION FOR SMAPVEX16-MB CAMPAIGN

		#	VV				VH			
			R2 (%)	RMSE (rad)	Bias (rad)	StDv (rad)	R2 (%)	RMSE (rad)	Bias (rad)	StDv (rad)
Configuration1 (ΔM_v, Δb)	**wheat**	37	39.7	1.12	0.20	1.12	19.6	1.48	-0.15	1.49
	canola	36	42.5	1.09	-0.31	1.06	19.6	1.41	-0.37	1.38
	corn	37	27.4	1.25	0.21	1.25	13.9	1.48	-0.54	1.40
	soybean	36	40.3	1.06	0.25	1.05	20.9	1.41	0.30	1.40
	bare	38	67.7	0.78	0.07	0.79	54.3	0.97	0.05	0.98
Configuration2 (ΔM_v, Δh)	**wheat**	37	43.9	1.09	-0.05	1.10	25.9	1.37	-0.18	1.38
	canola	36	46.9	0.97	-0.22	0.96	23.1	1.22	0.15	1.23
	corn	37	38.2	1.18	-0.14	1.19	13.7	1.34	-0.13	1.35
	soybean	36	45.8	1.03	0.35	0.99	13.6	1.48	-0.28	1.47
	bare	38	76.9	0.66	0.03	0.67	59	0.92	-0.07	0.92

TABLE VI
ACCURACY OF THE MODEL REGULATION FOR THE CANEX-SM10 CAMPAIGN

	#	**HH**				**VH**				**VV**			
		R2 (%)	**RMSE (rad)**	**bias (rad)**	**StDv (rad)**	**R2 (%)**	**RMSE (rad)**	**Bias (rad)**	**StDv (rad)**	**R2 (%)**	**RMSE (rad)**	**Bias (rad)**	**StDv (rad)**
wheat	32	53.5	0.94	0.32	0.89	38.1	1.04	0.36	0.99	52.4	0.76	0.31	0.70
canola	33	55.8	1.26	-0.81	0.99	41	1.04	-0.38	0.99	55.1	0.99	-0.44	0.90
weeds	13	56.9	0.79	-0.33	0.75	40	1.29	-0.49	1.24	52.7	0.69	0.38	0.60
peas	14	49.6	0.91	0.41	0.84	41	1.05	-0.42	0.99	53.1	0.92	0.31	0.90
bare	32	72.9	0.61	-0.02	0.62	55.6	0.57	0.13	0.56	69	0.38	0.06	0.38

accdjusted model's accuracy in both configurations is presented in Table V for the SAMPVEX16-MB campaign. The explanatory power of the regression model is greatest for bare fields in both configurations (Table V). Comparing different polarizations, it is observed that the regression model provides better results for the VV polarization than VH in both configurations. These results are the consequences of the less correlation between φ and ΔM_v in their scatter-plots of the VH polarization.

Comparing the two configurations, the calibration of the configuration 2 ($\beta_{\Delta M_v}$ and $\beta_{\Delta \mathrm{h}}$) provides more reliable results, indicating that the Δh, as ΔV descriptor in (4), was modeled better than Δb. However, (4) could not accurately model ΔV for both configurations in C-band, especially over corn field (RMSE of 1.48 rad, bias of 0.54 rad), because this band is highly affected by ΔV. Comparing different crops in Table V, the regression model provides better results for canola and soybean, and wheat with R^2 of 46.9%, 45.8%, 43.9%, and RMSE(bias) of 0.97($-$0.22), 1.18($-$0.14), and 1.09($-$0.05) rad, respectively.

In summary, it is concluded that configuration 2 [i.e., using Δh as ΔV in (4)] provides better results compared to configuration 1 [i.e., using Δb as ΔV in (4)]. Therefore, configuration 2 is only considered in the following process.

Fig. 11 shows a comparison between the estimated φ using linear regression and the obtained φ of the interferograms for the CanEx-SM10 campaign. Table VI also shows the model regression accuracy for different crop types. In this campaign, like the SMAPVEX16-MB campaign, the regression model provided better results for the bare fields (RMSE = [0.38 $-$ 0.61] rad, R^2 = [55% $-$ 72%], bias = [0.02 $-$ 0.06], and StDv = [0.38 $-$ 0.62] rad, depending on the polarization types). Comparing different polarizations, the results of the VV and HH polarizations have better accuracy (RMSE = [0.38 $-$ 0.99] rad, R^2 $-$ [49% - 72%], bias = [0.02 $-$ 0.44] rad, and StDv = [0.38 $-$ 0.9] rad, depending on the land cover types). The lower accuracy in the VH polarization is due to the low correlation in the previous results. Because of using L-band in the CanEx-SM10 campaign, the results show better accuracy than the SAMPVEX16-MB campaign (C-band) for vegetation fields, which is due to more penetration of L-band than C-band. The differences and errors are discussed in Sections VI-F and VI-G. Other insignificant changes (e.g., little changes in vegetation, wind condition, and atmospheric condition) have more effects on C-band, which causes the correlation and estimation accuracy to decrease more. For example, RMSE (StDv) varying from 0.38 (0.38) to 1.04 (0.9) rad and from 0.78 (0.79) to 1.48 (1.49) rad were obtained for L-band and C-band, respectively.

D. Accuracy Assessment of the $\boldsymbol{\Delta M_v}$ Estimation

The estimated ΔM_v using the adjusted regression model was compared to the *in situ* data for investigating the potential of the model to estimate ΔM_v from the φ. As discussed, because of the better results of configuration 2 ($\beta_{\Delta M_v}$ and $\beta_{\Delta \mathrm{h}}$) for SMAPVEX16-MB campaign, the processing and analysis are only conducted for the configuration Δh and ΔM_v.

The estimated and *in situ* ΔM_v are compared for each field and for each polarization to compute the statistical indices (see Figs. 12 and 13). The regression model worked well for ΔM_v estimation over bare fields for both campaigns (with lowest RMSE, bias, and StDv), which indicates valuable information of φ for ΔM_v estimation. Comparing the results obtained for the

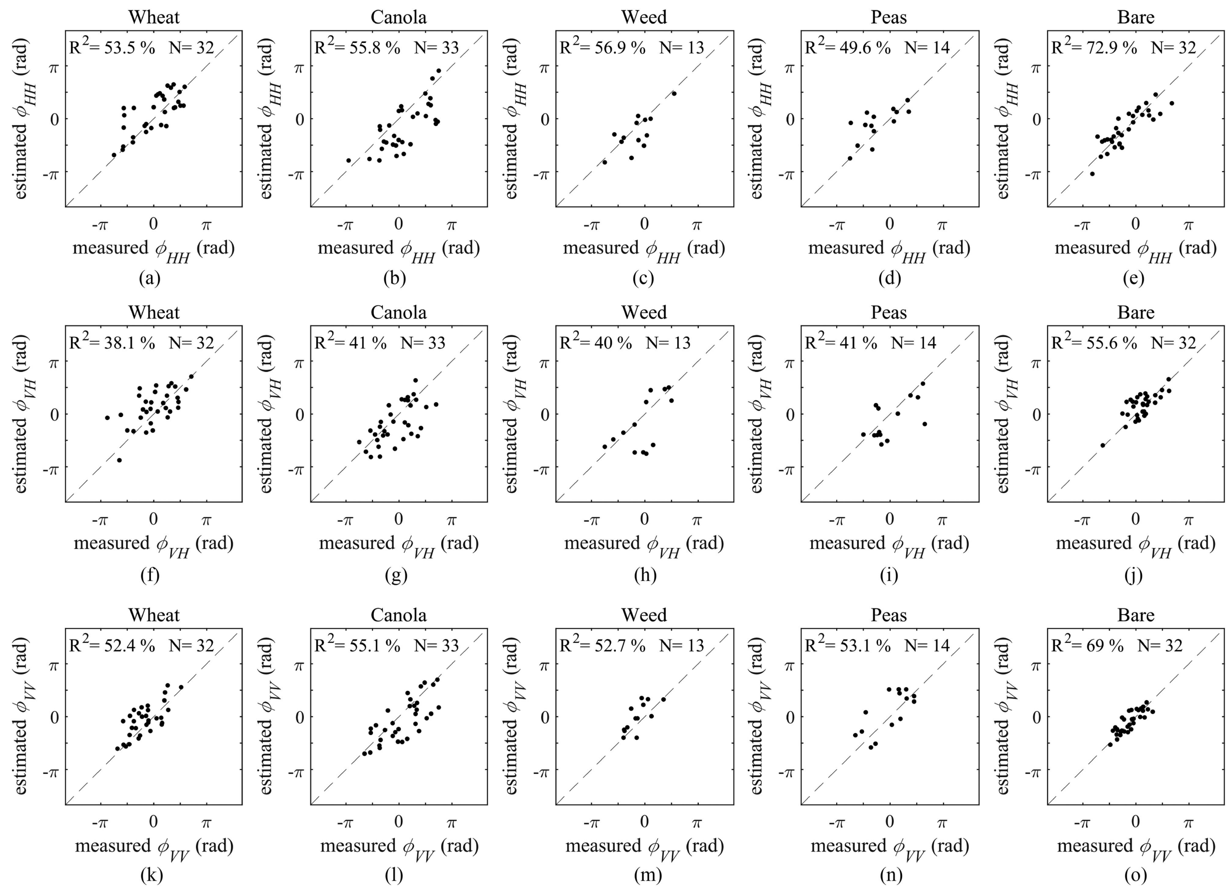

Fig. 11. Regression between the estimated and measured φ over the CanEx-SM10 campaign.

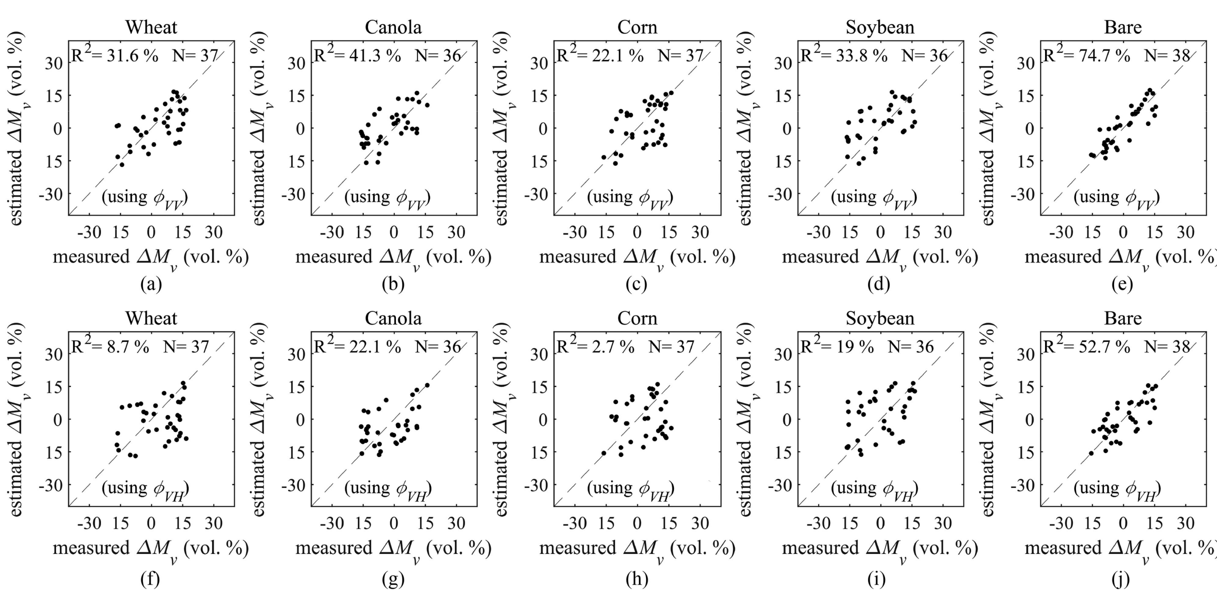

Fig. 12. Regression between the estimated and measured ΔM_v over the SMAPVEX16-MB campaign.

two campaigns, the model also provided more reliable results for the vegetated fields in L-band, which is due to longer wavelength and very short ΔT. For the SMAPVEX16-MB campaign, the results of the canola and soybean fields provided promising accuracy. However, the model did not generally provide reliable results over vegetated fields in C-band. The lowest accuracy is related to the vegetated fields in C-band (See Table VII). Finally, comparing different polarizations shows that the copolarizations φ_{HH} and φ_{VV} are more suitable for ΔM_v estimation.

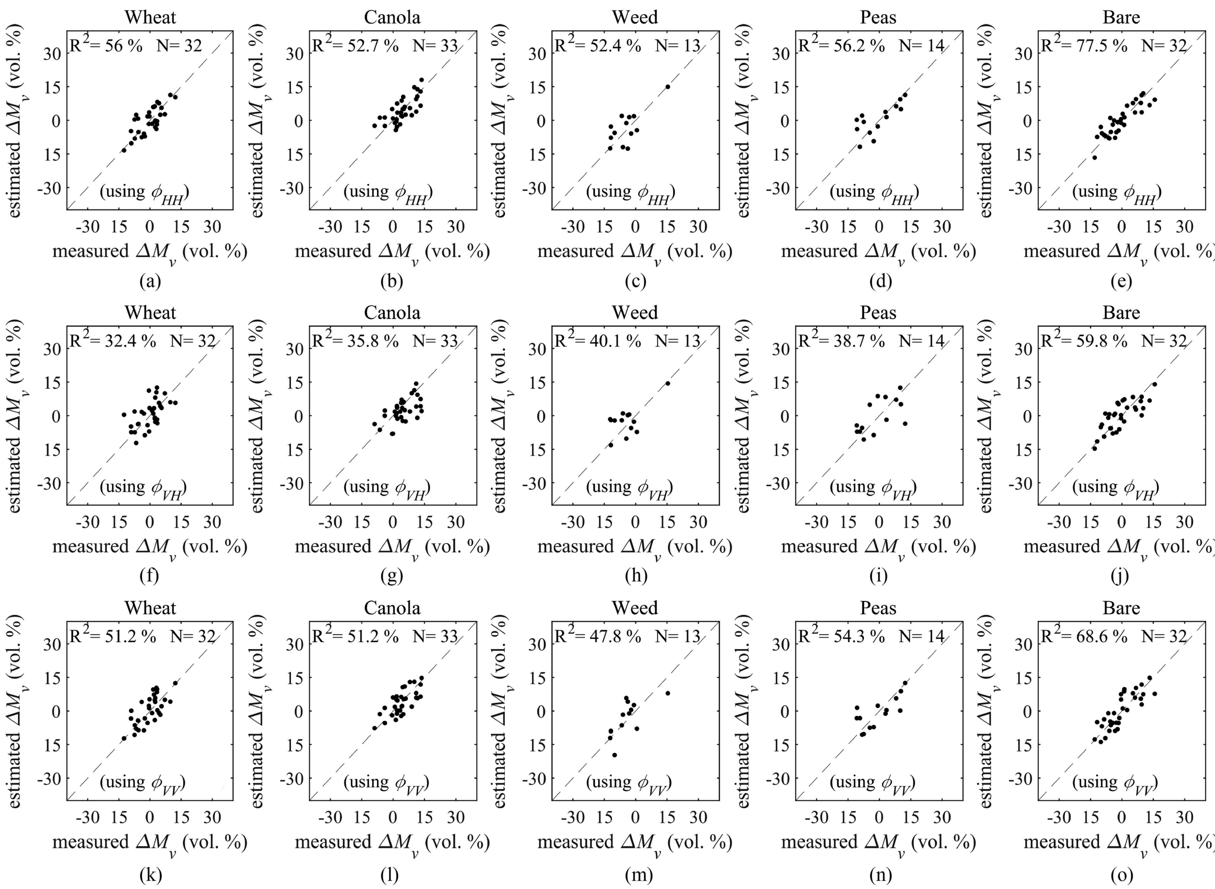

Fig. 13. Regression between the estimated and measured ΔM_v over the CanEx-SM10 campaign.

TABLE VII
ACCURACY OF ΔM_v ESTIMATION USING φ AND THE REGRESSION MODEL

		SMAPVEX16-MB				**CanEx-SM10**		
		VV	VH			VV	VH	HH
wheat	R2 (%)	31.6	8.70	wheat	R2 (%)	56	32.4	51.2
	RMSE (vol. %)	9.35	12.19		RMSE (vol. %)	4.11	5.52	4.68
	bias (vol. %)	-2.37	-4.39		bias (vol. %)	0.160	0.810	0.700
	StDv (vol. %)	9.17	11.53		StDv (vol. %)	4.17	5.55	4.70
Canola	R2 (%)	41.3	22.1	Canola	R2 (%)	52.7	35.8	51.2
	RMSE (vol. %)	8.19	9.29		RMSE (vol. %)	4.09	5.24	4.19
	bias (vol. %)	2.89	-1.12		bias (vol. %)	0.07	-2.06	-0.45
	StDv (vol. %)	7.77	9.35		StDv (vol. %)	4.16	4.89	4.23
Corn	R2 (%)	22.1	2.70	Weeds	R2 (%)	52.4	40.1	47.8
	RMSE (vol. %)	9.34	11.91		RMSE (vol. %)	5.43	6.12	5.87
	bias (vol. %)	-1.20	-2.95		bias (vol. %)	0.95	2.03	0.85
	StDv (vol. %)	9.39	11.69		StDv (vol. %)	5.56	6.01	6.05
Soybean	R2 (%)	33.8	19	Peas	R2 (%)	56.2	38.7	54.3
	RMSE (vol. %)	9.29	11.27		RMSE (vol. %)	5.42	6.73	5.49
	bias (vol. %)	2.30	2.35		bias (vol. %)	0.95	0.38	-0.29
	StDv (vol. %)	9.13	11.18		StDv (vol. %)	5.54	6.98	5.69
Bare	R2 (%)	74.7	52.7	Bare	R2 (%)	77.5	59.8	68.6
	RMSE (vol. %)	4.67	6.38		RMSE (vol. %)	3.50	4.76	4.46
	bias (vol. %)	0.25	-0.34		bias (vol. %)	0.18	0.52	0.27
	StDv (vol. %)	4.73	6.46		StDv (vol. %)	3.55	4.81	4.53

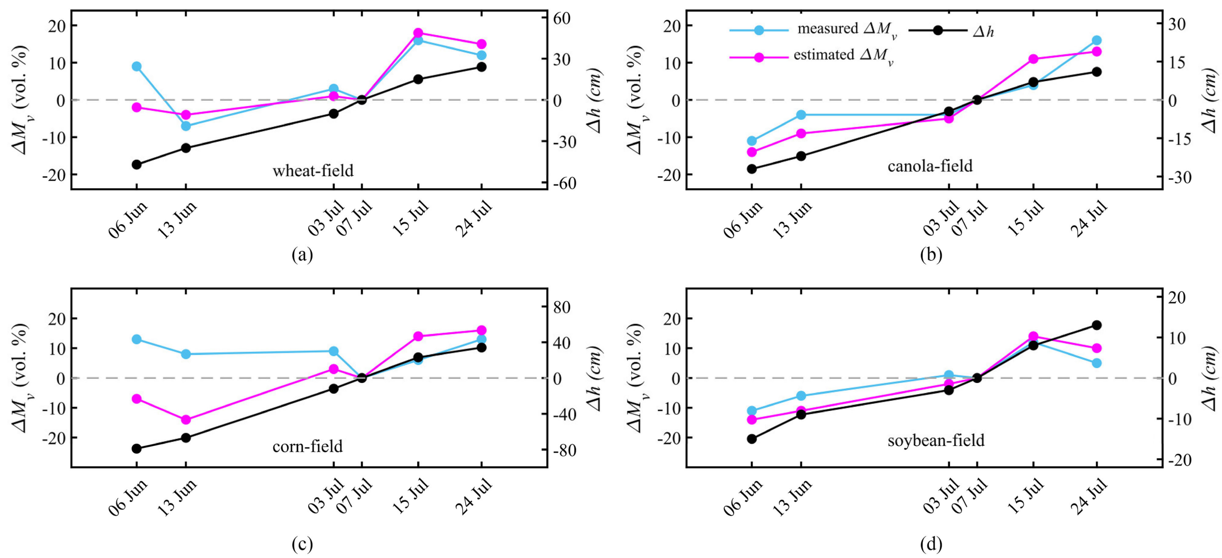

Fig. 14. Temporal changes of Δh, ΔM_v, φ, and the estimated ΔM_v for a sample over (a) wheat, (b) canola, (c) corn, and (d) soybean fields.

E. Differences Between Polarizations

Although ΔM_v and ΔV have similar effects on all the polarizations, various polarizations behave differently with those changes, which is because of scattering characteristics of different polarizations [35], [36], [44], [45]. For example, it was observed that the cross-polarization φ_{VH} variations have less correlation with changes in ΔM_v compared to the correlation of variations of the copolarizations φ with ΔM_v. These results are consistent with the results reported in [10] and [14]. Various polarizations behave differently for different crop types. For the SMAPVEX16-MB campaign, the coefficients associated with the wheat field or other crop types are different in the VV and VH polarizations. According to the two configurations for this campaign (Fig. 9), $\beta_{\Delta V}$ is also different for various configurations in each polarization. In the estimation process for the CanEx-SM10 campaign (i.e., L-band data), the estimated coefficients of the regression model in the VV and HH polarizations behaved similarly, but the values of the coefficients in the HH polarization is more than the ones in the VV polarization. For this campaign, the coefficients associated with the VH polarization have more variability, which shows instability in the relationship between φ_{VH} and ΔM_v.

More reliable results and accuracy are associated with the VV and HH polarizations in the accuracy assessment section. The VH polarization presents unstable results for both campaigns, which can be due to the lower correlation in the γ and φ scatter-plots. Comparing the copolarization results for the two campaigns, the VV polarisation results over the SMAPVEX16-MB campaign showed lower accuracy, which is due to the higher frequency of C-band and more ΔT in the SMAPVEX16-MB campaign.

F. Differences Between Crop Types

In this article, the effects of different vegetation covers are investigated for the SMAPVEX16-MB campaign (C-band) in more details. Various vegetation covers affect the φ differently, which leads to having various effects in ΔM_v estimation. Since configuration 2 (Δh and ΔM_v) in the SMAPVEX16-MB campaign provides better results, the focus of this section is on vegetation height changes. Fig. 14 shows temporal changes of vegetation height, ΔM_v, φ, and estimated ΔM_v using the regression model. According to this figure, it is observed that the efficiency of the regression model is highly dependent on how Δh and ΔM_v change. For example, according to Fig. 14(b) and (d), the model provided better results when Δh and ΔM_v behave similarly. However, Fig. 14(a) and (c) show the model was not reliable for different changes in Δh and ΔM_v. By comparing the estimated and measured ΔM_v in Fig. 14(b), especially on June 13, 2016, it is observed that the model does not provide reliable results with the high vegetation change rates. In fact, higher vegetation growth rate and further plant growth lead to lower accuracy of the regression model. For example, the correlation between ΔM_v and φ for the wheat and corn fields are less than those of canola and soybean fields due to their higher growth rate.

Comparing the accuracy of ΔM_v estimation for different crops in Fig. 12 (SMAPVEX16-MB campaign) and according to Fig. 14, the regression model was failed for ΔM_v estimation in the corn and wheat fields with long ΔT in C-band. The model was also unable to provide reliable results in other crop fields (e.g., canola and soybean) over the SMAPVEX16-MB campaign because of long ΔT and high-frequency data (C-band). However, Fig. 13 shows that the model provides reliable results with acceptable accuracy for ΔM_v estimation for the L-band. This is because of $\Delta T < 11$ days and higher penetration. Consequently, the results show that the linear regression model was not able to model plant changes. In fact, a large error entered in the ΔM_v estimation for high ΔV and its high rate.

G. Sources of Errors

The φ is not only affected by ΔM_v but also by all changes that occurred during the ΔT which can reduce the correlation between φ and ΔM_v and causes more errors in ΔM_v estimation using the regression model. In this section, the errors that are related to the phase component, which was not considered in the modeling, are first discussed. Then, the errors associated with the type of modeling (e.g., modeling of φ as a simple regression function of ΔM_v and ΔV) are discussed.

In this article, the components of φ_{def}, $\varphi_{\mathrm{topo\_res}}$, $\varphi_{\mathrm{atm\_d}}$, $\varphi_{\mathrm{orb\_d}}$, and φ_{noise} were considered insignificant and negligible, and they were not considered in the regression model [see (1)] to reduce the complexity of the DInSAR equation. However, it is worth noting that noise samples' effect was reduced by identifying noisy samples, which decrease correlation using the statistical filter. The error of removing the DEM component ($\varphi_{\mathrm{topo\_res}}$) depends on the accuracy of the DEM and the DEM resolution. This error can change φ [46], [47]. The error caused by atmospheric delay ($\varphi_{\mathrm{atm\_d}}$) depends on the conditions and water vapor in the atmosphere, and this error has effects on the φ signal [48]–[50]. This error also depends on the sensor frequency (i.e., more severe for lower frequencies) [6], [51]. According to the purpose of this study, there were some periods of precipitation during ΔT in both case studies, which causes a change in the atmospheric conditions, and, thus, reduces the correlation between ΔM_v and φ.

The regression model has an error in estimating ΔM_v over the vegetated areas due to linear modeling and ignoring some effective parameters. According to the fact that the vegetation coefficients of the model were estimated separately for each field and for both configurations of the SMAPVEX16-MB campaign, the results showed that the model was not able to model plant changes accurately in C-band, causing errors in ΔM_v estimation. Changing in wind speed and direction, especially in areas with vegetation cover, also reduces the correlation between φ and ΔM_v, which is due to changes in physical conditions of vegetation. This error for vegetation with higher height reduces the correlation between φ and ΔM_v, due to the greater impact on the plants. Consequently, the linear regression model was not able to accurately estimate ΔM_v over the vegetated fields for long ΔT and in high frequencies (C-band). However, for the CanEx-SM10 campaign, the model provides reliable results for the vegetated fields, which is due to the longer wavelength of the L-band ($\sim$24 cm) and the very short ΔT. These results are consistent with previous studies (e.g., [9], [10], and [21]).

VII. Conclusion

In this article, the estimation of ΔM_v using φ observation was investigated in the C-band of Sentinel-1 satellite data over the SAMPVEX16-MB campaign and in the L-band of the UAVSAR airborne data over the CanEx-SM10 campaign. We applied a linear regression model to establish the relationship between ΔM_v and φ. The results showed that the model could accurately estimate ΔM_v over bare fields for short ΔT, where the deformation and other changes that depend on ΔT are negligible. However, the results were not appropriate for the vegetated fields, especially for the SMAPVEX16-MB campaign, where the data were at high frequencies (C-band). Comparing the data from two campaigns, L-band provided better results of ΔM_v estimation in the vegetated fields due to the invisibility of vegetation changes for longer wavelengths, such as L-band in shorter ΔT (shorter than 11 days). In general, the regression model could not accurately model vegetation changes, which caused more errors in the results of the SMAPVEX16-MB campaign because of the significant effects of ΔV on the C-band and the lack of proper modeling of ΔV effects.

Errors in this research that reduced the accuracy of ΔM_v estimation, are listed into three groups: 1) The initial assumptions; 2) lack of proper modeling of the effects of ΔV in the regression model; 3) lack of modeling of the effective parameters, such as roughness, swelling behavior, and wind changes. However, the results showed that it would be feasible to use 6-day Sentinel-1 interferograms to monitor M_v over bare fields. Moreover, future SAR missions, such as NASA-ISRO SAR Mission (NISAR), or Hydroterra would provide multifrequency data or short spatiotemporal baseline, which are more suitable for monitoring M_v. Furthermore, the results showed that ΔM_v could be estimated using φ for $\Delta T > 25$ days with an average RMSEs of 5 and 7.5 vol. % over bare fields and vegetation areas, respectively. Comparing InSAR technique to other microwave methods for M_v monitoring, which are based on physical models or backscatter ratios, using radar intensity or backscatter ratios provide more promising accuracy, especially for M_v change detection over vegetation areas [11], [52].

We demonstrated that φ has adequate information to estimate ΔM_v for short spatiotemporal baselines, especially for longer wavelengths, such as L-band. The linear regression model can provide reliable results over bare fields in the C-band and L-band for all the polarization. However, this model cannot properly model ΔV effects on φ, especially in C-band (lower penetration), causing unreliable results for ΔM_v estimation over vegetation fields.

Acknowledgment

The authors would like to thank all the members of the SMAPVEX16-MB and CanEx-SM 2010 campaigns for collecting and providing these valuable datasets. The authors would also like to thank European Space Agency (ESA) for providing the Sentinel-1 datasets, which are also available through Copernicus Open Access Hub. Additionally, they would like to thank Dr S. Zwieback for his valuable technical feedback on this article, which has significantly improved this article. Finally, the authors thank the four anonymous reviewers and the IEEE JSTARS editorial team for their valuable feedback, which has improved this article.

References

[1] L. Liu, T. Zhang, and J. Wahr, "InSAR measurements of surface deformation over permafrost on the North Slope of Alaska," *J. Geophysical Res. Earth Surf.*, vol. 115, no. F3, 2010, Art. no. F03023.

[2] D. L. Galloway and J. Hoffmann, "The application of satellite differential SAR interferometry-derived ground displacements in hydrogeology," *Hydrogeol. J.*, vol. 15, no. 1, pp. 133–154, 2007.

[3] R. F. Hanssen, *Radar Interferometry: Data Interpretation and Error Analysis*, Berlin, Germany: Springer, 2001.

[4] D. Massonnet, P. Briole, and A. Arnaud, "Deflation of Mount Etna monitored by spaceborne radar interferometry," *Nature*, vol. 375, no. 6532, pp. 567–570, 1995.

[5] D. Massonnet *et al.*, “The displacement field of the Landers earthquake mapped by radar interferometry,” *Nature*, vol. 364, no. 6433, pp. 138–142, 1993.

[6] R. F. Hanssen, T. M. Weckwerth, H. A. Zebker, and R. Klees, “High-resolution water vapor mapping from interferometric radar measurements,” *Science*, vol. 283, no. 5406, pp. 1297–1299, 1999.

[7] R. Bürgmann, P. A. Rosen, and E. J. Fielding, “Synthetic aperture radar interferometry to measure Earth’s surface topography and its deformation,” *Annu. Rev. Earth Planet. Sci.*, vol. 28, no. 1, pp. 169–209, 2000.

[8] F. De Zan, A. Parizzi, P. Prats-Iraola, and P. López-Dekker, “A SAR interferometric model for soil moisture,” *IEEE Trans. Geosci. Remote Sens.*, vol. 52, no. 1, pp. 418–425, Jan. 2014.

[9] F. De Zan and G. Gomba, “Vegetation and soil moisture inversion from SAR closure phases: First experiments and results,” *Remote Sens. Environ.*, vol. 217, pp. 562–572, 2018.

[10] S. Zwieback, S. Hensley, and I. Hajnsek, “Assessment of soil moisture effects on L-band radar interferometry,” *Remote Sens. Environ.*, vol. 164, pp. 77–89, 2015.

[11] S. Ranjbar, A. Zarei, M. Hasanlou, M. Akhoondzadeh, J. Amini, and M. Amani, “Machine learning inversion approach for soil parameters estimation over vegetated agricultural areas using a combination of water cloud model and calibrated integral equation model,” *J. Appl. Remote Sens.*, vol. 15, no. 1, 2021, Art. no. 018503.

[12] B. Barrett, P. Whelan, and E. Dwyer, “Detecting changes in surface soil moisture content using differential SAR interferometry,” *Int. J. Remote Sens.*, vol. 34, no. 20, pp. 7091–7112, 2013.

[13] A. K. Gabriel, R. M. Goldstein, and H. A. Zebker, “Mapping small elevation changes over large areas: Differential radar interferometry,” *J. Geophys. Res. Solid Earth*, vol. 94, no. B7, pp. 9183–9191, 1989.

[14] S. Zwieback, S. Hensley, and I. Hajnsek, “Soil moisture estimation using differential radar interferometry: Toward separating soil moisture and displacements,” *IEEE Trans. Geosci. Remote Sens.*, vol. 55, no. 9, pp. 5069–5083, Sep. 2017.

[15] K. Morrison, J. C. Bennett, M. Nolan, and R. Menon, “Laboratory measurement of the DInSAR response to spatiotemporal variations in soil moisture,” *IEEE Trans. Geosci. Remote Sens.*, vol. 49, no. 10, pp. 3815–3823, Oct. 2011.

[16] G. Nesti *et al.*, “Phase shift and decorrelation of radar signal related to soil moisture changes,” in *Proc. 2nd Int. Workshop Retrieval Bio-Geo-Phys. Parameter SAR Data Land Appl.*, 1998, pp. 423–430.

[17] J.-P. Rudant, A. Bedidi, R. Calonne, D. Massonnet, and G. Nesti, “Laboratory experiments for the interpretation of phase shift in SAR interferograms,” *ESA SP*, 1997.

[18] Q. Yin, W. Hong, Y. Li, and Y. Lin, “Analysis on soil moisture estimation of SAR data based on coherent scattering model,” in *EUSAR 2014; 10th Eur. Conf. on Synthetic Aperture Radar*, 2014, pp. 1-4.

[19] I. Hajnsek and P. Prats, “Soil moisture estimation in time with D-InSAR,” in *Proc. IEEE Int. Geosci. Remote Sens. Symp.*, 2008, vol. 3, pp. III-546–III-549.

[20] M. Nolan, D. R. Fatland, and L. Hinzman, “DInSAR measurement of soil moisture,” *IEEE Trans. Geosci. Remote Sens.*, vol. 41, no. 12, pp. 2802–2813, Dec. 2003.

[21] B. Barrett, P. Whelan, and E. Dwyer, “The use of C-and L-band repeat-pass interferometric SAR coherence for soil moisture change detection in vegetated areas,” *Open Remote Sens. J.*, vol. 5, pp. 37–53, 2012.

[22] S. Hensley *et al.*, “Effect of soil moisture on polarimetric-interferometric repeat pass observations by UAVSAR during 2010 Canadian soil moisture campaign,” in *Proc. IEEE Int. Geosci. Remote Sens. Symp.*, 2011, pp. 1063–1066.

[23] Y. Eshqi Molan and Z. Lu, “Can InSAR coherence and closure phase be used to estimate soil moisture changes?,” *Remote Sens.*, vol. 12, no. 9, 2020, Art. no. 1511.

[24] S. Cloude, *Polarisation: Applications in Remote Sensing*. Oxford, U.K.: Oxford Univ. Press, 2009.

[25] R. Bamler and P. Hartl, “Synthetic aperture radar interferometry,” *Inverse Problems*, vol. 14, no. 4, 1998, Art. no. R1.

[26] S. R. Cloude and K. P. Papathanassiou, “Polarimetric SAR interferometry,” *IEEE Trans. Geosci. Remote Sens.*, vol. 36, no. 5, pp. 1551–1565, Sep. 1998.

[27] V. Brancato and I. Hajnsek, “Separating the influence of vegetation changes in polarimetric differential SAR interferometry,” *IEEE Trans. Geosci. Remote Sens.*, vol. 56, no. 12, pp. 6871–6883, Dec. 2018.

[28] D. Massonnet and K. L. Feigl, “Radar interferometry and its application to changes in the Earth’s surface,” *Rev. Geophys.*, vol. 36, no. 4, pp. 441–500, 1998.

[29] P. S. Agram and M. Simons, “A noise model for InSAR time series,” *J. Geophys. Res. Solid Earth*, vol. 120, no. 4, pp. 2752–2771, 2015.

[30] P. Beckmann and A. Spizzichino, *The Scattering Of Electromagnetic Waves From Rough Surfaces*. Oxford, U.K.: Pergamon Press, 1987.

[31] S. Zwieback and I. Hajnsek, “Influence of vegetation growth on the polarimetric zero-baseline DInSAR phase diversity—Implications for deformation studies,” *IEEE Trans. Geosci. Remote Sens.*, vol. 54, no. 5, pp. 3070–3082, May 2016.

[32] H. McNairn *et al.*, “SMAPVES-16 Experimental Plan,” Jet Propulsion Lab., California Inst. Technol., Pasadena, CA, USA, 2016. [Online]. Available: https://smap.jpl.nasa.gov/science/validation/fieldcampaigns/SMAPVEX16/

[33] R. Magagi *et al.*, “Canadian experiment for soil moisture in 2010 (CanEx-SM10): Overview and preliminary results,” *IEEE Trans. Geosci. Remote Sens. ,* vol. 51, no. 1, pp. 347–363, Jan. 2013.

[34] A. G. Fore *et al.*, “UAVSAR polarimetric calibration,” *IEEE Trans. Geosci. Remote Sens.*, vol. 53, no. 6, pp. 3481–3491, Jun. 2015.

[35] Z. Akhavan, M. Hasanlou, M. Hosseini, and H. McNairn, “Decomposition-based soil moisture estimation using UAVSAR fully polarimetric images,” *Agronomy*, vol. 11, no. 1, 2021, Art. no. 145.

[36] M. T. Hallikainen, F. T. Ulaby, M. C. Dobson, M. A. El-Rayes, and L.-K. Wu, “Microwave dielectric behavior of wet soil-Part 1: Empirical models and experimental observations,” *IEEE Trans. Geosci. Remote Sens.*, vol. 23, no. 1, pp. 25–34, Jan. 1985.

[37] N. R. Peplinski, F. T. Ulaby, and M. C. Dobson, “Dielectric properties of soils in the 0.3-1.3-GHz range,” *IEEE Trans. Geosci. Remote Sens.*, vol. 33, no. 3, pp. 803–807, May 1995.

[38] M. Foumelis, “ESA snap Sentinel-1 toolbox,” Eur. Space Agency, Paris, France, 2017. [Online]. Available: https://sentinel.esa.int/web/sentinel/toolboxes/sentinel-1

[39] G. G. Hamedani and M. N. Tata, “On the determination of the bivariate normal distribution from distributions of linear combinations of the variables,” *Amer. Math. Monthly*, vol. 82, no. 9, pp. 913–915, 1975.

[40] A. Genz and F. Bretz, *Computation of Multivariate Normal and t Probabilities*. Berlin, Germany: Springer, 2009.

[41] L. Tsang and J. A. Kong, *Scattering of Electromagnetic Waves: Advanced Topics*. Hoboken, NJ, USA: Wiley, 2004.

[42] J. Pinheiro, D. Bates, S. DebRoy, D. Sarkar, and R. C. Team, “Linear and nonlinear mixed effects models,” *R Package Version*, vol. 3, no. 57, pp. 1–89, 2007.

[43] A. Zarei, R. Shah-Hosseini, S. Ranjbar, and M. Hasanlou, “Validation of non-linear split window algorithm for land surface temperature estimation using Sentinel-3 satellite imagery: Case study; Tehran Province, Iran,” *Adv. Space Res.*, vol. 67, pp. 3979–3993, 2021.

[44] F. Ulaby and D. Long, *Microwave Radar and Radiometric Remote Sensing*. Ann Arbor, MI, USA: Univ. Michigan Press, 2014.

[45] E. Khedri, M. Hasanlou, and A. Tabatabaeenejad, “Semi-analytical soil moisture retrieval using PolSAR imagery,” in *Proc. IEEE Int. Geosci. Remote Sens. Symp.*, 2017, pp. 4897–4900.

[46] H. A. Zebker and R. M. Goldstein, “Topographic mapping from interferometric synthetic aperture radar observations,” *J. Geophysical Res. Solid Earth*, vol. 91, no. B5, pp. 4993–4999, 1986.

[47] R. M. Goldstein and C. L. Werner, “Radar interferogram filtering for geophysical applications,” *Geophysical Res. Lett.*, vol. 25, no. 21, pp. 4035–4038, 1998.

[48] R. Goldstein, “Atmospheric limitations to repeat-track radar interferometry,” *Geophysical Res. Lett.*, vol. 22, no. 18, pp. 2517–2520, 1995.

[49] H. A. Zebker, P. A. Rosen, and S. Hensley, “Atmospheric effects in interferometric synthetic aperture radar surface deformation and topographic maps,” *J. Geophysical Res. Solid Earth*, vol. 102, no. B4, pp. 7547–7563, 1997.

[50] P. R. Rowntree, “Large-scale land-atmosphere models and data needs,” in *Proc. ESA/NASA Int. Workshop*, 1995, pp. 3–15.

[51] R. Klees and D. Massonnet, “Deformation measurements using SAR interferometry: Potential and limitations,” *Geologie en Mijnbouw*, vol. 77, no. 2, pp. 161–176, 1998.

[52] D. Palmisano, A. Balenzano, G. Satalino, F. Mattia, N. Pierdicca, and A. Monti-Guarnieri, “Sentinel-1 sensitivity to soil moisture at high incidence angle and its impact on retrieval,” in *Proc. Int. Geosci. Remote Sens. Symp.*, 2018, pp. 1430–1433.

Sadegh Ranjbar received the B.Eng. degree in surveying and geomatics engineering from the Faculty of Civil Engineering, Shaheed Rajaei Teacher Training University, Tehran, Iran, in 2017, and the M.Eng. degree in remote sensing from the College of Engineering, University of Tehran, Tehran, Iran, in 2021.He is currently working toward the master graduate degree in remote sensing.

He has worked on various remote sensing applications, including but not limited to soil moisture estimation, watershed management, land cover/land use classification, natural hazard detection, and change detection. His research interests include analyzing different remote sensing datasets through AI and ML approaches for urban and agro-environmental applications.

Mehdi Akhoondzadeh received the B.Sc. degree in civil-surveying engineering from the Amirkabir University of Technology, Tehran, Iran, in 2002, and the M.Sc. and Ph.D. degrees in civil-remote sensing engineering from the University of Tehran, Tehran, Iran, in 2005 and 2011, respectively.

He is currently an Assistant Professor with the School of Surveying and Geo-Spatial Engineering, College of Engineering, University of Tehran. His research interests include applied remote sensing, soft computing, time series analysis, anomaly detection, and earthquake precursors.

Brian Brisco received the B.Sc. degree in ecology and the M.Sc. degree in soil science from the University of Guelph, Guelph, ON, Canada, in 1977 and 1981, respectively, and the Ph.D. degree in remote sensing/physical geography from The University of Kansas, Lawrence, KS, USA, in 1985.

He is an internationally recognized authority on synthetic aperture radar (SAR) and its application to a wide range of environmental monitoring applications. Since 1975, he has been involved in remote sensing, and from 1977 to 1980, he participated in the SURSAT Project before spending four years with the Remote Sensing Laboratory, The University of Kansas, under the supervision of Dr. F.T. Ulaby, widely recognized as one of the world's leading authorities on radar. From 1989 to 1997, he was with Intera, Austin, TX, USA, as a Research Associate after completion of an NSERC Postdoctoral Fellowship from the Canada Centre for Remote Sensing. From 1997 to 2004, he was with Noetix Research Inc., Ottawa, ON, Canada, where he was the Director of Research and Applications Development. In 2004, he joined CCRS as a Research Scientist. He has authored or coauthored extensive publications on vegetation characterization, crop identification and monitoring, conservation farming or soil erosion mapping, soil moisture estimation, land cover mapping, wetland mapping, rangeland management, forestry, and developing tools, and techniques for ground truth data acquisition. He has authored or coauthored more than 200 publications, including more than 50 peer-reviewed journal publications and is the author of two chapters in the *Manual of Remote Sensing* (ASPRS) volume on radar applications. His work has included experience with interferometry, polarimetry, and radar backscatter modeling including software development and operational implementation. His research focuses on using remote sensing, particularly synthetic aperture radar (SAR), for mapping and managing renewable resources.

Dr. Brisco provides peer review services to all the major remote sensing journals and participates as an external examiner for many graduate students at various universities in Canada and abroad. He has been consulted or contracted by government and nongovernment organizations on a wide range of SAR applications and system development, including NRCan, CSA, DND, AAFC, EC, NASA, ESA, NASDA, NOAA, USDA, and CAS. He has extensive contacts in the SAR community worldwide and has worked in China, Vietnam, Malaysia, Thailand, Indonesia, South Africa, Argentina, Uruguay, Chile, Brazil, Columbia, and Costa Rica. He was the recipient of the Past-President of the Canadian Remote Sensing Society and the Canadian Aeronautics and Space Institute.

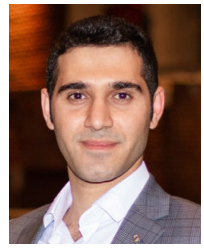

Meisam Amani (Senior Member, IEEE) received the B.Eng. degree in geomatics engineering from the University of Tabriz, Tabriz, Iran, in 2012, the M.Eng. degree in remote sensing engineering from the K.N. Toosi University of Technology, Tehran, Iran, in 2014, and the Ph.D. degree in electrical engineering from the Memorial University of Newfoundland, St. John's, NL, Canada, in 2018.

He is currently a Senior Remote Sensing Scientist and the Key Specialty Leader of data analytics with a global consulting and engineering company, called Wood PLC, Aberdeen, U.K., where he manages and leads various academic, governmental, and industrial remote sensing projects worldwide. He worked on different applications of remote sensing, including but not limited to land cover or land use classification, soil moisture estimation, drought monitoring, water quality assessment, watershed management, power or transmission line monitoring, fog detection and nowcasting, and ocean wind estimation. He has utilized various remote sensing datasets and different machine learning and big data processing algorithms.

Dr. Amani is currently an Associate Editor for the IEEE JOURNAL OF SELECTED TOPICS IN APPLIED EARTH OBSERVATIONS AND REMOTE SENSING and the lead Guest Editor for a special issue in *Remote Sensing*. He is also a regular Reviewer in about 15 international remote sensing journals.

Mehdi Hosseini received the B.Eng. degree in surveying engineering from the University of Science and Technology, Arak, Iran, in 2003 and the M.Eng. and Ph.D. degrees in remote sensing engineering from the University of Tehran, Tehran, Iran, in 2005 and 2011, respectively.

He is currently Associate Research Professor with the NASA Harvest Hub, Department of Geographical Sciences, University of Maryland, College Park, MD, USA. His research related to optical and SAR applications to crop monitoring and production forecasting for both large scale agricultural systems and smallholder systems at the field to national scales. This involved developing and refining models for yield forecasting, cropland and crop type mapping, and crop condition assessments. He has expertise in model development for environmental applications using radar and optical remote sensing data. During 2017–2019, he was a Co-leader of an international project involving 18 countries for studying the best practices for crop biomass and leaf area index (LAI) estimations and crop type classification using synthetic aperture radar (SAR). His research interests include using physical, statistical and machine learning approaches for modeling agricultural, and environmental parameters.